Journal of Nuclear Materials 119 (1983) 1–25
North-Holland, Amsterdam

MECHANISMS OF HELIUM INTERACTION WITH RADIATION EFFECTS IN METALS AND ALLOYS: A REVIEW *

L.K. MANSUR and W.A. COGHLAN **

Metals and Ceramics Division, Oak Ridge National Laboratory Oak Ridge, Tennessee 37830, USA

Received 10 June 1983; accepted 23 June 1983

Helium has been shown to cause major changes in the radiation effects response of metals and alloys. Examples are described. Physical mechanisms underlying these effects are discussed in terms of the theory of radiation effects. An extended treatment of the critical cavity radius concept is developed. Several new analytical results are presented. Applications are reviewed covering the temperature extension of swelling by gas, the evolution of bimodal cavity size distributions and the necessity for gas as a prerequisite to swelling under some conditions. The effect of helium on the dose dependence of swelling is described in terms of its effects on the balance of point defect sink strengths. Mechanisms underlying the enhanced formation and growth of cavities on precipitates when helium is present are discussed. A proposal is described to explain recently observed large effects of helium on phase stability.

1. Introduction

A widely appreciated generalization of the results of research in radiation effects is that the type and severity of radiation induced changes are highly dependent on alloy composition. An impurity that must be singled out because of its extreme potency and because of its unavoidable production in transmutation reactions during neutron irradiation is the insoluble rare gas helium. In charged particle irradiation experiments helium is often injected deliberately to study its role in radiation effects evolution. Helium is produced to levels of tens of parts per million in typical high dose fast reactor irradiations and to levels of thousands of parts per million under the conditions anticipated in future fusion reactors. Since the displacement rates in these two types of reactors are expected to be comparable, helium can be thought of as one of the agents by which the large differences in neutron spectra manifest themselves. Studies of helium interactions with displacement effects are therefore of particular relevance to fusion reactor materials research.

A rich variety of phenomena has been discovered in the study of radiation-induced changes in microstructure, solute segregation, and phase stability. Understanding these phenomena is leading to new insights into materials behavior and to principles for the design of more radiation resistant materials. In particular, development of mechanistic descriptions of helium and displacement effects interactions is an active area of current research. The theory of radiation effects based on point defect reactions, developed for swelling, irradiation creep, phase stability, and to a more limited extent in other areas has been extended to include helium effects. Through this framework numerous reaction pathways become evident. In the present paper we review and develop several mechanisms of helium interaction with the evolution of structural and compositional microheterogeneity. The emphasis primarily is on swelling, with some discussion of phase instability and solute segregation. The underlying theory will be described using analytic results for simplicity wherever possible. Results on phase instability are quite recent and have mainly been observed in complex alloys. For these reasons many of the results have not yet come under as detailed theoretical scrutiny, and no attempt is made to review this area completely. Several areas are highlighted and qualitative proposals regarding these phenomena are discussed.

* Research sponsored by the Division of Materials Sciences, US Department of Energy under contract W-7405-eng-26 with the Union Carbide Corporation. This paper is based on an invited presentation at the TMS-AIME symposium on Radiation Damage Analysis and Fusion Reactors, October 24–28, 1982, St. Louis, Mo., USA.

** Present address: Department of Mechanical and Aerospace Engineering, Arizona State University, Tempe, Arizona 85287, USA.

2. Helium effects

A primary contribution of the theory of radiation effects is that it reveals how virtually all kinetic processes occurring during irradiation are interdependent. On a more detailed level it gives a quantitative tool with which to evaluate results of interest such as swelling, creep, segregation, and so forth. Before delving into selected aspects we can describe several modes of action under which various identifiable processes fall. These modes may be classified as cavity pressurization, microstructural changes, microcompositional changes, and changes in atomic transport. Most changes ascribable to cavity pressurization center around helium-induced variations in the critical size for bias-driven cavity growth. Effects of helium on microstructural sink strength may change markedly the dose dependence of swelling. In alloys, changes in the composition on a local scale may be caused by irradiation. Helium may affect changes in precipitation and solute segregation. Finally, the presence of helium may affect point defect transport as well as solute transport. The first three areas will be discussed in this paper. Certain aspects of the last have been discussed in another paper [1]. Of course these modes of helium effects are interactive and overlapping and this division, though useful in understanding underlying mechanisms, is not rigid. In fact all these modes may be viewed to be related in part through the common feature of helium trapping at vacancies and vacancy clusters [2].

3. The critical cavity radius

3.1. Background

In a material containing several types of point defect sinks, such as dislocations and cavities, for example, the sinks generally have different capture efficiencies for vacancies and interstitials. During irradiation there will be therefore unequal partitioning of point defects to sinks. The difference in capture efficiencies responsible for this is termed the bias which has a mathematical definition detailed below. The sense of the bias results in a larger flux of vacancies to voids and of interstitials to dislocations. However, the thermal emission rate of vacancies from cavities goes as $\exp(\text{radius}^{-1})$ and, for realistic vacancy formation energies, goes as $\exp(\text{temperature}^{-1})$. At a given temperature there is therefore a critical cavity radius above which the bias-induced net vacancy influx is larger than the net thermal vacancy outflux and below which the converse is true. Similarly at a given cavity radius there is a critical temperature below which the bias-induced net vacancy influx is larger than the net thermally emitted vacancy outflux. As the temperature is raised the critical radius increases. Similarly, for larger cavity radius the critical temperature is larger.

The theory of cavity growth based on point defect reactions in its earliest forms harbored the existence of a critical cavity radius [3–5]. An essentially similar critical radius concept was developed earlier in calculations of gas bubble growth in fissile materials [6]. Similarly, in the theory of cavity nucleation [7], the existence of a critical cavity radius is a central concept. There the critical radius corresponds to a maximum in the kinetic analog of free energy in an irradiated material.

Brailsford and Bullough [8] have introduced the related concept of a critical stress for stress driven breakaway swelling. For a given stress this also can be translated to a critical radius. However, the physical origin of that critical radius is different from the one considered here. There it arises because the void absorbs a net vacancy flux provided by sources, such as dislocations and grain boundaries, that emit enhanced vacancy fluxes under stress.

Sears [9] apparently first gave a discussion of the critical cavity radius and related quantities and provided analytic expressions based on an ideal gas. Odette and co-workers [10] in their calculations of cavity growth in the presence of helium pointed out that some cavities would not grow above a critical cavity size if they contained less than a certain number of gas atoms. Hayns et al. [11] explored the critical radius further. They demonstrated through numerical solutions of the governing differential equations that the critical radius had an exponential temperature dependence. An explicit expression was also given for the critical radius, which did not include gas pressure, gave simplified temperature and dose rate dependencies, and covered sink-dominated regimes. Ghoniem and Gurol [12] gave a more accurate expression with respect to temperature dependence, neglecting gas pressure and point defect recombination.

Fisher et al. [13] gave an expression similar to that of ref. 11 but including the gas pressure in the form of an ideal gas law. Recently, Townsend [14] obtained a relatively simple implicit expression for critical cavity radius. This result utilizes a modified Van der Waals equation of state, gives a more accurate temperature dependence and neglects point defect recombination. This work was combined with the results of Spitznagel et al. [15] who developed methods to relate measured cavity size distributions to material parameters in order to extract lower

bound estimates of critical cavity radii from dual-ion irradiation experiments. Hishinuma and Mansur [16] gave a simple implicit expression for both the ideal and Van der Waals gases with accurate dose rate and temperature dependences, valid for arbitrary recombination fraction, and including the effect of gas pressure. The solution of this equation was used to develop a cavity stability map and to discuss the common occurrence of bimodal cavity distributions in experiments where helium is present during irradiation. The important related concept of a critical number of contained gas atoms has been elucidated, chiefly by Sears [9], by Russell [7], and by Odette and co-workers [10,17] in their work on mechanisms and rates of cavity nucleation. In the present paper we review and derive several new results for critical radius and for related quantities.

The critical radius may also be applied to develop other predictions of interest. For example, for a given set of conditions the critical radius may be found. Then one of the conditions, say dose rate, microstructure, or gas pressure may be varied independently. With the requirement that the critical radius remain fixed, the necessary change in any one of the other conditions, say temperature, may then be determined. This was the approach of Mansur, and of Hayns and Mansur in derivations of the temperature shifts of cavity growth with dose rate and microstructure [18], and of the temperature extension of cavity growth with gas pressure [19], respectively.

3.2. Theory

3.2.1. Framework

The spatially independent and quasi-steady-state forms of the rate equations of point defect continuity suffice for the present work. More complete forms of these equations and their reduction to simpler forms are described elsewhere [20].

The continuity equations may be written as

$$G_v - RC_vC_i - K_vC_v = 0, \tag{1}$$

$$G_i - RC_vC_i - K_iC_i = 0. \tag{2}$$

Subscripts v and i denote vacancies and interstitials. The G's are the point defect generation rates per unit volume and include contributions from radiation and thermal processes, given by

$$G_v = fG(1-\epsilon_v) + G_T, \tag{3}$$

$$G_i = fG(1-\epsilon_i) + G\epsilon_i', \tag{4}$$

where f is the fractional effective point defect generation rate accounting for mutual recombination within the cascade, and G is the displacement rate. The symbols ϵ account for the further fractional reduction of the effective generation rate by in-cascade clustering of like point defects. The quantity ϵ_i' is the additional fractional interstitial production due to injected interstitials when the situation under study is a self-ion bombardment experiment.

The thermal vacancy generation rate is denoted by G_T and can be written

$$G_T = D_vC_v^0 \sum_j \xi_v^j Z_v^j S^{0j}. \tag{5}$$

Here $D_v = D_v^0 \exp(-E_v^m/kT)$ is the vacancy diffusion coefficient, where D_v^0 is a constant, E_v^m is the vacancy migration energy, k is Boltzmann's constant and T is absolute temperature. The bulk thermal equilibrium vacancy concentration is given by

$$C_v^0 = \Omega^{-1} \exp\left(S_v^f/k\right) \exp\left(-E_v^f/kT\right), \tag{6}$$

where Ω is atomic volume and S_v^f and E_v^f are respectively the entropy and energy of vacancy formation. The quantity ξ^j, the thermal emission factor, relates the thermal vacancy concentration near a sink of type j to the bulk thermal equilibrium concentration. For cavities this is given by

$$\xi^c = \exp\left[-\left(P_g - \frac{2\gamma}{r_c}\right)\Omega/kT\right], \tag{7}$$

where P_g is the gas pressure within the cavity, γ is the surface tension, and r_c is the cavity radius. For dislocation network we take $\xi^d = 1$. In eq. (5) the symbol Z_v^j denotes the capture efficiency of sink type j for vacancies. Later we also use the analogous symbol Z_i^j for interstitials. The symbol S^{0j} is the ideal diffusional sink strength of sink type j [21]. The derivation of S^{0j} disregards elastic interactions between point defect and sink, rate limitations at the sink–matrix interface and multiple sink interactive effects. In this formalism, these "non-idealities" are subsumed in the factors Z_v^j and Z_i^j. For cavities $S^{0c} = 4\pi r_c N_c$, where N_c is the cavity concentration. For dislocations $S^{0d} = Z^{0d}L$, where Z^{0d} is the prefactor in the ideal case and L is the dislocation density. The derivations of the Z's from diffusional and elastic formulations is an active subfield of radiation effects research. In eqs. (1) and (2) $K_{i,v}$ denote overall loss rates of point defects to sinks

$$K_{i,v} = D_{i,v} \sum_j Z_{i,v}^j S_{i,v}^{0j},$$

and $R = 4\pi r_r(D_i + D_v)$ is the coefficient of recombination, where r_r is the radius of recombination.

After having specified the material and irradiation

parameters entering these equations we solve eqs. (1) and (2) for the point defect concentrations [4,5,20]. The results are given as physical (i.e., per unit volume) concentrations

$$C_v = \frac{[K_i K_v + R(G_i - G_v)]}{2RK_v} \times \left[\left(1 + \frac{4RG_v K_i K_v}{[K_i K_v + R(G_i - G_v)]^2}\right)^{1/2} - 1\right] \quad (8)$$

and

$$C_i = \frac{[K_i K_v + R(G_v - G_i)]}{2RK_i} \times \left[\left(1 + \frac{4RG_i K_i K_v}{[K_i K_v + R(G_v - G_i)]^2}\right)^{1/2} - 1\right]. \quad (9)$$

Here $D_i = D_i^0 \exp(-E_i^m/kT)$ is the interstitial diffusion coefficient where D_i^0 is a constant and E_i^m is the interstitial migration energy. From these concentrations the growth rate of a cavity is determined by the net vacancy flux,

$$\frac{dr_c}{dt} = \frac{\Omega}{r_c}[Z_v^c D_v C_v - Z_i^c D_i C_i - Z_v^c D_v C_v^e(r_c)]. \quad (10)$$

The symbol $C_v^e(r_c)$ denotes the thermal vacancy concentration near a cavity of radius r_c and, as stated in eq. (7), it is given by

$$C_v^e(r_c) = C_v^0 \exp\left[-\left(P_g - \frac{2\gamma}{r_c}\right)\frac{\Omega}{kT}\right]. \quad (11)$$

The above analysis envisions point defects and extended sinks only. When low order mobile point defect clusters and higher order point defect clusters created directly in cascades or by diffusional agglomeration are to be included, the size of the set of eqs. (1) and (2) must be expanded to describe continuity of each species (see ref. 1, for example).

3.2.2. Critical cavity radius

From the forms of eqs. (10) and (11) it can be anticipated that there may be zeros in the cavity growth rate as the cavity radius is varied. The largest root beyond which there are no further zeros in dr_c/dt is defined as the critical radius. Above this the cavity grows indefinitely by bias-driven growth.

The computation of the critical radius is accomplished by substituting eqs. (8), (9) and (11) into eq. (10). The cavity radius r_c is varied to find the roots $dr_c/dt = 0$. Fig. 1 illustrates the results of calculations of this type for cases with various numbers of contained gas atoms in the cavity. The values of the parameters used in these and subsequent computations in this paper are given in table 1. The results depend on the equation of state used to relate the number of contained gas atoms to the gas pressure. In the present paper we consider two possible equations of state. The first is the ideal gas equation

$$P_g = 3n_g kT/4\pi r_c^3, \quad (12)$$

where n_g is the number of gas atoms in a cavity of radius r_c. The second is the modified Van der Waals

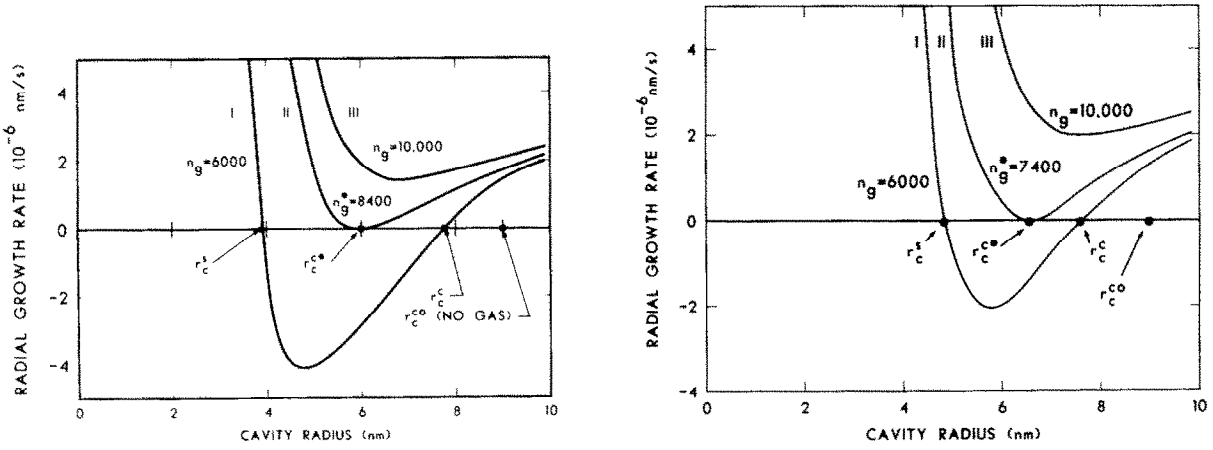

Fig. 1. Plot of cavity growth rate versus cavity radius. Plot on the left uses ideal gas and plot on the right uses Van der Waals equation of state. The dose rate is 10^{-6} dpa/s at 610°C.

Table 1
Values of important materials parameters used in calculations

E_v^m(eV)	E_i^m(eV)	E_v^f(eV)	γ(J/m^2)	B(m^3/atom)	Ω(m^3)	Bias (%)	r_r(nm)	L(m^{-2})
1.2	0.15	1.6	1	1.59×10^{-29}	1.09×10^{-29}	5	0.4	5×10^{14}

equation of state which is given by

$$P_g = n_g kT/\left(\tfrac{4}{3}\pi r_c^3 - n_g B\right), \tag{13}$$

where B is the Van der Waals volume correction coefficient. Fig. 1 shows the behavior of dr_c/dt versus r_c, for these two cases.

It can be seen that when the number of contained gas atoms is small there are two roots. This case is labeled as curve I. These roots can be denoted r_c^s and r_c^c, where the s superscript denotes that a cavity at that size is stable and the c superscript denotes the critical cavity radius. A cavity with a fixed number of gas atoms that is beyond its corresponding r_c^s but below r_c^c will shrink back to r_c^s. A cavity below r_c^s with that same number of gas atoms will grow to r_c^s and stop. A cavity above r_c^c with this same number of gas atoms will continue to grow to larger radii without limit, by bias-driven growth. Such a cavity could arrive above its r_c^c corresponding to its n_g by fluctuations, by a temperature change or other changes in irradiation conditions. If the number of contained gas atoms is large enough there will be no intersections with the $dr_c/dt = 0$ axis. This case is labeled as curve III. Cavities containing such numbers of gas atoms do not have a physically meaningful critical radius. There is effectively no size below which they will not grow by bias driven growth. At some critical number of gas atoms, which depends on conditions such as temperature, dose rate, and materials parameters, there will be just one intersection of the function dr_c/dt versus r_c with the axis $dr_c/dt = 0$. This case is labeled as curve II. The corresponding number of gas atoms we denote as n_g^* and the corresponding minimum critical radius, where r_c^s and r_c^c coincide, we denote as r_c^{c*}. The quantity n_g^* is the corresponding maximum number of gas atoms that may be contained in a cavity for there to still exist a critical radius. At n_g^* the critical cavity radius is at its minimum finite value r_c^{c*}. Above n_g^* the cavity will have no barrier to bias driven growth no matter how small it is. This type of plot of the behavior of critical cavity radius with gas content was described by Sears [9] and Odette and Langley [10], and employed more recently by Townsend [14].

Explicit expressions will be derived for r_c^{c0} (no gas), r_c^{c*}, n_g^*, and the gas pressure P_g^* corresponding to r_c^{c*} and n_g^*. In the steady-state the fluxes of vacancies and interstitials to all sinks must be equal. This condition is expressed as

$$D_v\left(\bar{Z}_v C_v - \overline{\xi Z}_v C_v^0\right) = D_i \bar{Z}_i C_i, \tag{14}$$

where

$$\bar{Z}_{i,v} = \sum_j Z_{i,v}^j S^{0j} / \sum_j S^{0j}, \tag{15}$$

is the weighted average of the sink capture efficiencies. The factor $\overline{\xi Z}_v$ is similarly defined as the weighted average of the product of the thermal emission factor and the capture efficiency,

$$\overline{\xi Z}_v = \sum_j \xi^j Z_v^j S^{0j} / \sum_j S^{0j}. \tag{16}$$

The interstitial formation energy in materials of interest is so high as to make the thermal interstitial counterpart to C_v^0 negligible.

The analysis is simplified considerably when we assume that dislocations, cavities, and mutual recombination represent the only point defect loss processes, and further that dislocations are the dominant of the two sinks. Thus

$$Z_v^d L \gg 4\pi r_c N_c Z_v^c. \tag{17}$$

This assumption gives rise to the great simplification that C_v and C_i as well as G_T and the thermal vacancy concentration in the matrix are independent of cavity radius. Although this is the main departure from generality, it is not too restrictive physically. Condition (17) is generally fulfilled early in an irradiation where determination of the critical radius is usually of most interest; and it is often fulfilled throughout an irradiation, for example, in stainless steels irradiated in fast reactors (see later discussion of the dislocation dominated regime in the dose dependence of swelling). In view of relations (15), (16), and (17), eq. (14) becomes

$$Z_v^d D_v\left(C_v - C_v^0\right) = Z_i^d D_i C_i. \tag{18}$$

Setting $dr_c/dt = 0$ in eq. (10), substituting eqs. (18) and (11) into the resulting expression, taking logarithms and rearranging gives [16]

$$r_c = \frac{2\gamma}{P_g + \dfrac{kT}{\Omega}\ln\left((1-Z)\dfrac{C_v}{C_v^0} + Z\right)}. \tag{19}$$

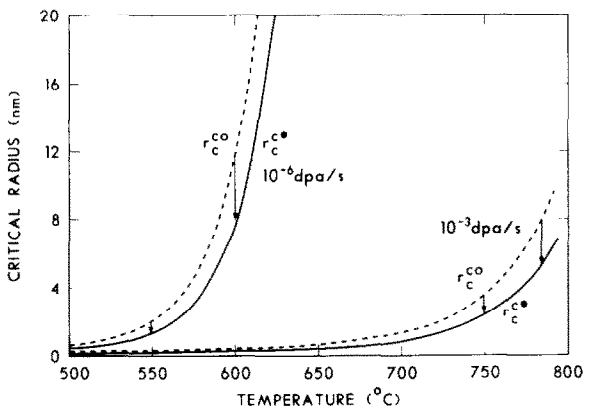

Fig. 2. Behavior of critical radius as a function of temperature. Solid curves show gas free critical radius, r_c^{c0}, while dashed curves show minimum critical radius with gas r_c^{c*}.

Here Z denotes the capture efficiency ratio $Z_i^c Z_v^d / Z_v^c Z_i^d$. This quantity substracted from unity as in eq. (19) is closely related to the bias, which we define [20,21] as $(Z_i^d Z_v^c - Z_v^d Z_i^c)$. The quantity Z has a second order dependence on microstructure.

If there is no contained gas in the cavity, $P_g = 0$, then eq. (19) gives directly the solution for the critical radius,

$$r_c^{c0} = \frac{2\gamma}{\frac{kT}{\Omega}\ln\left((1-Z)\frac{C_v}{C_v^0} + Z\right)}, \qquad (20)$$

where the 0 superscript denotes the gas-free case. Fig. 2 shows the behavior of r_c^{c0} as a function of temperature for several different displacement rates.

If there is gas in the cavity then P_g also is dependent on cavity radius as can be seen from eqs. (12) and (13). In this case eq. (19) does not yet give the explicit solution for the critical radius. To illustrate this we may plot both the left hand and right hand sides of eq. (19) as a function of actual cavity radius, r_c. Such a plot is shown in fig. 3. Fig. 3 represents a cavity stability map and illustrates the behavior of the critical radius in an alternative way to fig. 1 [16]. Three types of curves are shown labeled I, II, and III and these correspond to the three types of curves shown in fig. 1 labeled similarly. In general, for a fixed number of helium atoms, the gas pressure is high when the actual cavity radius is small. This results in a critical radius smaller than the actual radius reflecting the fact that thermal vacancy emission from the cavity is suppressed by high pressure. As the actual cavity radius increases, however, the pressure drops and the thermal vacancy emission rate increases. This is counteracted by the fact that a larger radius of curvature means an exponentially lower thermal vacancy emission rate, by eq. (11). Whether the actual radius ultimately reaches the critical radius depends upon the values of the irradiation and materials variables. In particular, whether or not this occurs is strongly dictated by the number of gas atoms contained in the cavity.

The horizontal line in the figure is the gas free

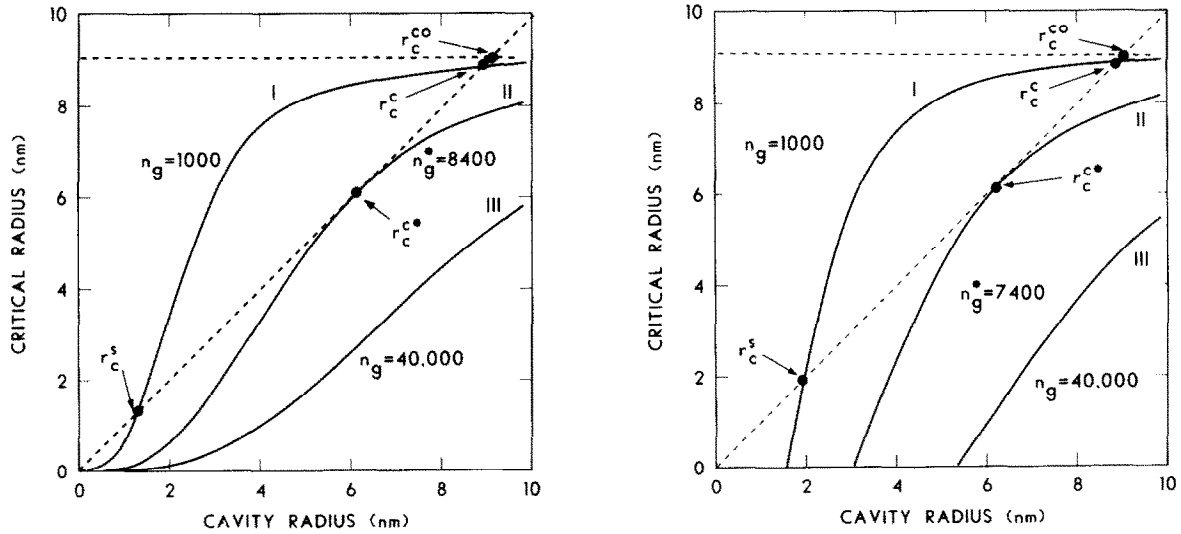

Fig. 3. Cavity stability map obtained from eq. (19). Plot on the left shows results for ideal gas and plot on the right shows results for Van der Waals gas equation of state. Dose rate is 10^{-6} dpa/s at a temperature of 610°C.

critical radius, r_c^{c0}. Curve I shows the situation where the critical radius would be larger than the actual radius except at very small sizes. The cavity embryos indicated by curve I cannot grow above the first intersection with the 45° line, a radius we designated earlier by r_c^s. This is one root of eq. (19). The other root is the second intersection of the curves at r_c^c. This is the critical cavity radius, above which cavities grow by bias-driven growth. The distance between r_c^s and r_c^c represents a barrier to growth which can be overcome by fluctuations in point defect arrival and emission or by continuing accumulation of gas atoms. In contrast, the cavity embryos indicated by curve III continue to grow because these cavities contain a large number of gas atoms. The critical radius therefore would be smaller than the actual cavity radius for all values of the actual cavity radius. There is thus no critical radius for these cavities and they grow indefinitely by bias-driven growth. A special case is where the number of gas atoms is just sufficient to cause the curve to be tangent to the 45° line at only one point of intersection. Only cavities with this particular number of gas atoms, or fewer, can persist during the irradiation without shrinkage or growth. This size corresponds to r_c^{c*}, the coincidence of r_c^s and r_c^c. It represents the minimum possible critical radius. The number of gas atoms n_g^* associated with r_c^{c*} represents the maximum number of gas atoms a cavity can contain and still exhibit a critical radius. Fig. 3 (left) corresponds to ideal gas behavior while fig. 3 (right) corresponds to the Van der Waals gas. The shapes of the curves are different but the intersections, r_c^c, r_c^{c*}, and r_c^s are relatively insensitive to the gas equation of state used when the intersections are at large values. When the intersections are at small values, the intersections are sensitive to the equation of state used.

In fig. 4 we show the dependence of the critical radius, r_c^c, on the number of gas atoms n_g. For both gas laws the function r_c^c monotonically decreases with increasing n_g. At the value $n_g = n_g^*$ where $r_c^c = r_c^{c*}$ the critical radius vanishes.

Several analytical results can now be derived. First we treat the ideal gas. Substituting eq. (12) for P_g into eq. (19) and rearranging gives

$$g(r_c) = r_c^3 - \frac{2\gamma}{f} r_c^2 + \frac{3n_g kT}{4\pi f}, \tag{21}$$

where

$$f = \frac{kT}{\Omega} \ln\left((1-Z)\frac{C_v}{C_c^0} + Z\right).$$

We have denoted the expression by the function $g(r_c)$, which equals zero when r_c is one of the roots r_c^s or r_c^c. The condition that $g(r_c)$ be a minimum, i.e., that $dg(r_c)/dr_c = 0$, ensures that the two roots r_c^s and r_c^c are equal and defines the minimum critical radius r_c^{c*}. Taking the derivative of g with respect to r_c gives the second condition

$$\frac{dg(r_c)}{dr_c} = 3r_c^2 - \frac{4\gamma}{f} r_c. \tag{22}$$

Simultaneously setting eqs. (21) and (22) to zero permits us to solve for r_c^{c*}. The result is

$$r_c^{c*} = \frac{4\gamma\Omega}{3kT \ln\left((1-Z)\frac{C_v}{C_v^0} + Z\right)} \quad \text{(Ideal gas)}. \tag{23}$$

Comparing with the gas free critical radius, r_c^{c0}, of eq.

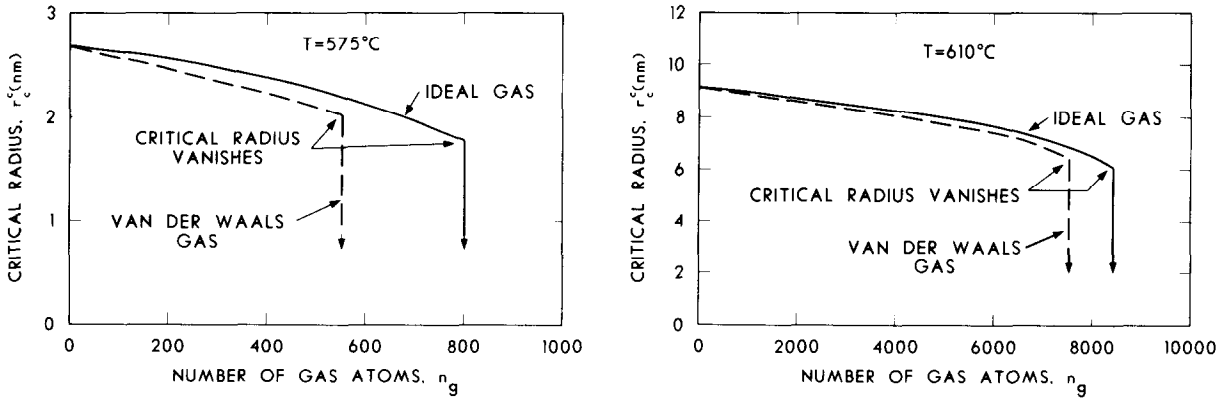

Fig. 4. The critical radius r_c^c as a function of the number of contained gas atoms n_g, for ideal and Van der Waals gas behavior, at 575 and 610°C.

(20) we see that the minimum finite critical radius that can be achieved with gas pressurization is given by

$$r_c^{c*}/r_c^{c0} = 2/3 \quad \text{(Ideal gas)}. \tag{24}$$

Fig. 2 shows how the minimum critical radius simply follows the gas-free critical radius in its temperature behavior.

Further interesting results follow from this analysis. An intermediate result leading to eq. (23) gives n_g^*,

$$n_g^* = \frac{128\pi\gamma^3\Omega^2}{81(kT)^3\left[\ln\left((1-Z)\dfrac{C_v}{C_v^0}+Z\right)\right]^2} \quad \text{(Ideal gas)}. \tag{25}$$

Sears [9] earlier obtained results similar to eqs. (23) and (25). In work on the nucleation of voids in metals, Russell [7] has derived similar expressions. Stoller and Odette [17] have also obtained similar forms. A minor difference is that the earlier results are expressed in terms of point defect arrival ratios while the results here are given in terms of sink capture efficiencies.

Now substituting eqs. (23) and (25) into eq. (12) we find that the pressure corresponding to the cavity of minimum critical radius r_c^{c*}, containing n_g^* gas atoms, is simply

$$P_g^* = \frac{kT}{2\Omega}\ln\left((1-Z)\frac{C_v}{C_v^0}+Z\right) \quad \text{(Ideal gas)}. \tag{26}$$

However, the equilibrium gas pressure corresponding to a cavity of size r_c^{c*} is

$$P_g^{eq} = 2\gamma/r_c^{c*}. \tag{27}$$

Substituting eq. (23) for r_c^{c*} we obtain

$$P_g^{eq} = \frac{3kT}{2\Omega}\ln\left((1-Z)\frac{C_v}{C_v^0}+Z\right) \quad \text{(Ideal gas)}. \tag{28}$$

Taking the ratio of eq. (26) to eq. (28) gives

$$P_g^*(r_c^{c*})/P_g^{eq}(r_c^{c*}) = 1/3 \quad \text{(Ideal gas)}. \tag{29}$$

This is a remarkably simple result. When enough gas has been added to the cavity to pressurize it to one third or more of its equilibrium pressure, at the size r_c^{c*}, then the cavity no longer exhibits a critical size. There will then be no barrier to bias-driven growth.

A similar approach to that described above and also yielding exact expressions has been worked out for the Van der Waals equation of state [22].

$$r_c^{c*} = \frac{4\gamma}{3f}\left[\tfrac{1}{2}\left(1-\frac{2Bf}{kT-Bf}\right)\left(1\pm\sqrt{1+\eta}\right)\right] \quad \text{(Van der Waals gas)}, \tag{30}$$

where

$$\eta = \frac{16B}{f(kT-Bf)}\Big/\left(\frac{8B/3}{(kT-Bf)}-\frac{4}{3f}\right)^2, \tag{31}$$

and

$$\eta_g^* = \frac{8\pi\gamma r_c^{c*2} - 16\pi f r_c^{c*3}/3}{kT-Bf} \quad \text{(Van der Waals gas)}. \tag{32}$$

The sign on the square root is determined by the physical requirement that the radius be positive. Similarly, the explicit expression for gas pressure is obtained directly by substituting eqs. (30)–(32) for n_g and r_c into eq. (13). These results are easily shown to reduce to those for the ideal gas as $B \to 0$. In general the results are numerically similar to those of the ideal gas for typical values of B, except when the cavity radii are small. The results of such comparisons can be seen graphically by inspection of figs. 1 and 3. Stoller and Odette [17] have also derived an implicit expression and cast it in a general analytic form to account for non-ideal gas effects, stress effects, and precipitate location by means of correction factors. Parker and Russell [23] gave approximations for the Van der Waals gas. Comparisons of the present results with those are described in ref. 22.

3.2.3. Critical radius in growth and nucleation theories

The above derivations and discussion are cast in the context of cavity growth theory. In the void swelling literature much of the discussion of the early stages of cavity formation has been in terms of nucleation theory. This theory was initially developed by Russell [24] and by Katz and Wiedersich [25] along the lines of classical precipitate nucleation theory with modifications to account for the new feature of simultaneous impingement of the precipitating "solute" (vacancy) and the solute which annihilates it (interstitial).

A fundamental formulation of vacancy clustering in terms of discrete master equations and their subsequent analytic approximation by a Fokker–Planck continuum representation gives a general description that includes both nucleation and growth [26–28]. The traditionally separated descriptions simply emphasize different regimes and processes within a more general framework. Nucleation theory is concerned primarily with determining cavity nucleation rates and densities, or probabilities of different trajectories through the space of vacancy and gas accumulation under irradiation conditions. Cavity growth theory is concerned primarily with describing

the kinetics of growth of an existing cavity population in response to an evolving microstructural environment. However, when required to describe precisely the same physical quantity both descriptions must give the same answer. We have already mentioned the work of Russell and co-workers [7,23] in arriving at similar expressions to those derived above. However, rather than simply make the statement that it is obvious that results must be equivalent, we show this in one case.

In nucleation theory the critical radius is determined by the condition that the kinetic analog of the free energy of the system containing the cavity is at its maximum. This is illustrated in fig. 5. In growth theory the critical radius is determined by the condition of zero net vacancy volume influx to the cavity. In Appendix A one condition is reduced to the other. This demonstrates that the critical radii, as well as the stable radii and the critical numbers of gas atoms, for a cavity containing an arbitrary number of gas atoms are equivalent in growth and nucleation theory.

3.3. Applications of the critical radius concept

The critical radius concept also can be applied to make further predictions about swelling behavior. Two aspects that are of interest are the predictions of temperature shifts and of the evolution of bimodal cavity size distributions.

3.3.1. Temperature shifts

Shifts in the temperature regime of void swelling may be brought about by changes in dose rate, changes in the microstructural environment and changes in gas pressurization. Fig. 6 is a schematic representation of the types of temperature shifts of swelling that are predicted by theory. Three types are shown corresponding to gas pressurization (top), different sink strengths (middle), and different dose rates (bottom). The shaded region of the upper figure, labeled gas assisted, is the temperature regime where gas assists cavities in achieving bias driven growth [29]. Below this the critical radii are small and gas is less important. Above this, the critical radii and n_g^* are so large that bias-driven growth is very difficult to achieve. Swelling occurs there by gas-driven bubble growth. Calculated dose rate and gas pressurization effects may be seen by inspection of fig. 2. At temperature $T^{(1)}$, say, and dose rate $G^{(1)}$, we see that the critical radius has a given value r_c^c. If temperature is increased to $T^{(2)}$, r_c^c becomes large very rapidly. Bias-driven swelling is therefore effectively not possible at high temperatures because cavities must first achieve

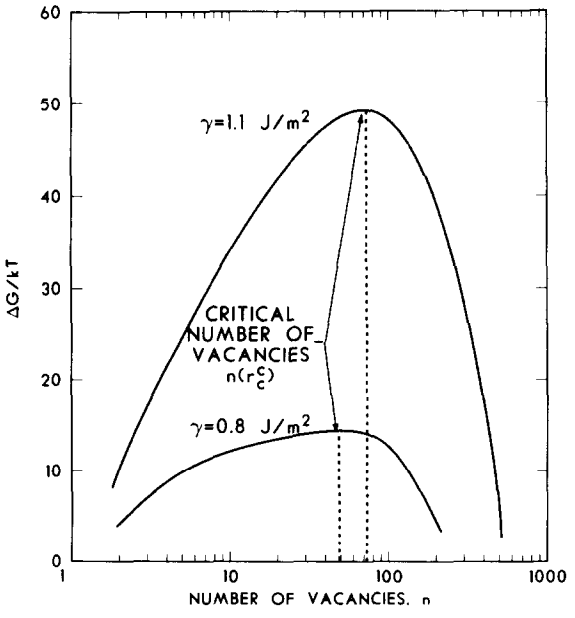

Fig. 5. Dependence of ΔG on the number of vacancies for two different values of the surface energy.

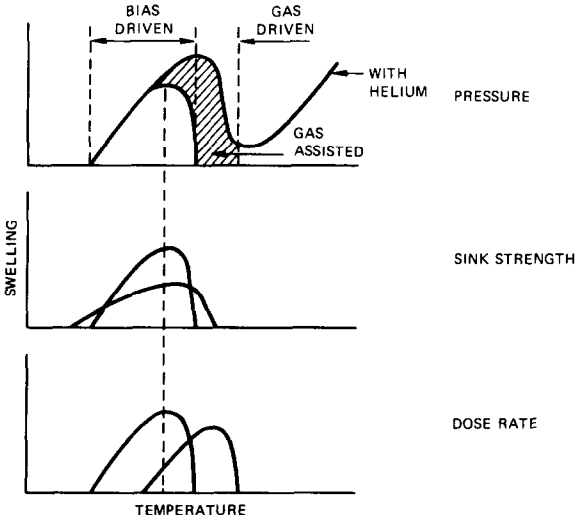

Fig. 6. Schematic illustration of three types of temperature shifts arising in the theory of swelling. The top figure shows the effect of gas pressurization in extending the temperature regime of swelling. The middle figure shows the effects of changes in sink strength in producing changes in temperature dependence, and the bottom figure shows the temperature shift caused by a change in dose rate.

the critical radius. However, if at the higher temperature the dose rate is increased to $G^{(2)}$, the magnitude of the critical radius is decreased and the same given value of r_c^c can be achieved at a higher temperature.

This temperature shift of void growth rate may be obtained by simply computing dr_c/dt versus T at two different dose rates from eq. (10) in conjunction with the auxiliary relations (8), (9), and (11). The curves will be displaced from each other in temperature and this gives directly the temperature shift. However, explicit analytical expressions for the temperature shift due to changes in dose rate may be obtained in certain limits. The procedure is based on eq. (10). When the third term in this equation equals the difference of the first two there will be no growth. Thus the ratio of the magnitudes of the third to the difference of the first two is unity. At a different dose rate it also holds that when the growth rate is zero the ratio is again unity, defining the corresponding condition at the new dose rate. These ratios may therefore be set equal to each other. More generally, in fact, the ratios need not equal unity but need simply equal each other. The result can be expressed as [20]

$$T^{(2)} - T^{(1)} = \frac{\dfrac{kT^{(1)2}}{E_v^m + n\left(E_v^f + E_v^*\right)} \ln\left(\dfrac{G^{(2)}}{G^{(1)}} \dfrac{M^{(1)}}{M^{(2)}}\right)}{1 - \dfrac{kT^{(1)}}{E_v^m + n\left(E_v^f + E_v^*\right)} \ln\left(\dfrac{G^{(2)}}{G^{(1)}} \dfrac{M^{(1)}}{M^{(2)}}\right)}. \tag{33}$$

In this equation E_v^* is the energy barrier, if any, in addition to the normal migration energy, that the vacancy must overcome on diffusing into the void. The symbols $M^{(1)}$ and $M^{(2)}$ are microstructural terms defined in ref. 18. The number n takes on values 1 to 2. If recombination is the chief mode of point defect loss, the value is 2, while if sinks dominate the value is 1. For a difference in dose rate of 10^3, roughly corresponding to the difference between neutron and ion irradiations, the temperature shift in stainless steels is of order 100–200°C.

The appearance of the quantities $M^{(1)}$ and $M^{(2)}$ signals an entirely separate physical basis of temperature shift. Even if $G^{(1)} = G^{(2)}$, there will be a temperature shift if the microstructural environments of the voids are different in conditions (1) and (2). The derivations and a tabulation of these results are given in ref. 18. For typical differences in dislocation density, for example, the temperature shift due to microstructural environment can be tens of degrees centigrade.

The temperature shift due to gas pressurization, really a temperature extension of the swelling regime in this case, rather than a shift of the entire swelling versus temperature plot, can be derived by similar methods. As seen from fig. 2 this result can be significant. For example, near 550°C at a dose rate of 10^{-6} dpa/s for the conditions employed in the calculations of fig. 2, the temperature shift due to gas pressurization is ~ 30°C. For a given temperature $T^{(1)}$ with no gas, the critical radius is a given value, r_c^c. If the temperature is raised to $T^{(2)}$ the critical radius increases by approximately 50%, from fig. 2, for a 30°C change about 550°C. However, if gas is added to change the pressure from $P^{(1)}$ to $P^{(2)}$ to the level n_g^* defined earlier, then the magnitude of the critical radius is reduced again to the given value of r_c^c. Of course as we discussed earlier the addition of more than n_g^* atoms of gas to a cavity essentially removes the critical radius.

Thus the critical radius concept is of great utility in understanding the temperature shifts of swelling with dose rate, microstructure, and gas pressure.

3.3.2. Bimodal cavity size distributions

Bimodal cavity size distributions are often observed in irradiated materials containing helium. See ref. 16 and references contained therein for example. Ref. 30 shows pronounced examples in the high nickel alloys. The typical bimodal distribution consists of a class of cavities of radii less than a few nanometers and another class of cavities spread about a much larger size, with relatively few cavities at the intermediate radii. Fig. 7 is an example observed in the work of Packan [31]. The experiment was a pulsed nickel ion irradiation of a pure stainless steel type material (Fe–17Cr–16.7Ni–2.5Mo) with simultaneous helium injection into the damaged region. Bimodal distributions were not observed in the absence of helium although significant swelling occurred.

The origin of the bimodal cavity distribution can be understood by reference to fig. 3. Early in dose in an irradiated material containing helium we visualize numerous cavity embryos that contain in general different numbers of helium atoms. The minimum critical radius is r_c^{c*}, corresponding to a number of contained gas atoms n_g^*. Cavities with less than n_g^* gas atoms cannot grow by bias driven growth and will persist at a size below r_c^{c*}, $r_c^{\flat}$, determined by where their trajectory of curve type I intersects the 45° line. Without fluctuations in point defect flux or accumulation of more helium, they cannot make the transition from their size $r_c^{\flat}$ to r_c^c required for bias driven growth. On the other hand, cavities either already having become larger than their corresponding critical size r_c^c by fluctuations, or

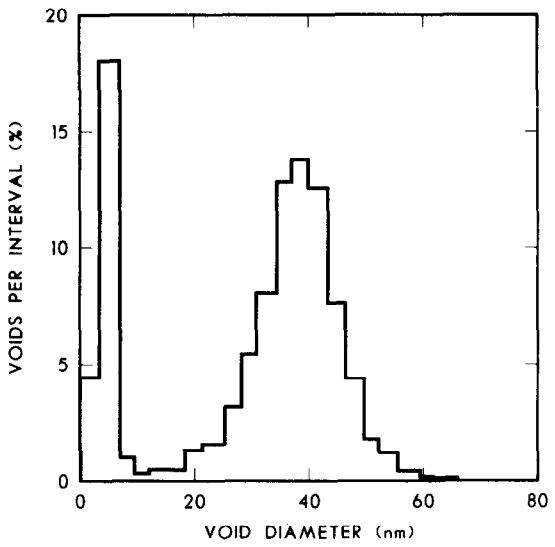

Fig. 7. Bimodal cavity size distribution observed in a "pure" stainless steel irradiated with nickel ions at 670°C to a dose of 10 dpa with the simultaneous injection of helium at a rate of 20 appm/dpa.

having accumulated more than n_g^* gas atoms, will grow indefinitely by bias-driven growth. These two different classes of cavities form the two different peaks in the bimodal distribution. The position of the upper peak depends directly on the dose. The position of the lower peak is defined such that its upper cutoff is equal to r_c^{c*}, i.e., to the radius where r_c^s and r_c^c coincide.

It is also worth mentioning at this point that r_c^s is in principle not the equilibrium bubble size, but is larger than that quantity, r_c^{eq}, defined by the condition where $r_c^{eq} = 2\gamma/P_g$. If an equilibrium bubble were put into a material under irradiation it would grow. At r_c^{c*} the relationship between r_c^s and r_c^{eq} can be deduced from eq. (29). If the bubble contained less than n_g^* gas atoms, it would ultimately stop at its r_c^s determined by its n_g. At stable radii significantly less than r_c^{c*}, the equilibrium bubble size r^{eq} and the stable cavity size, r_c^s, are more nearly equal, however. While irradiation is occurring with simultaneous helium production it is possible for some of the cavities in the smaller class of the bimodal cavity distribution to be promoted to bias-driven growth by accumulating more than n_g^* gas atoms.

Bimodal cavity size distributions in the presence of helium were predicted in the work of Odette and Frei [32]. Hayns and Wood [33] did an extensive series of calculations to evolve cavity size distributions for both diffusion limited and surface reaction limited growth kinetics. A prominent feature in these calcultions was the breakup of the initial distributions into bimodal distributions. Spitznagel et al. [15] have applied analyses of bimodal distributions extensively in interpreting their experimental results from dual ion irradiations.

To illustrate these points we have performed some simple calculations. Eq. (10) is generalized to become a set of equations each applying to a different radius group in a distribution. As the distribution evolves with dose we observe it to separate spontaneously into two size groups as anticipated. The distributions used in these calculations are chosen to be the simplest possible in order to show the effect most clearly. Some of the effects that we have considered previously when employing distributions in theoretical calculations have been intentionally omitted. For example, we have shown that cavity coalescence by impingement due to growth is important in changing the cavity size distribution as growth occurs [20,34]. Here cavitiy coalescence is omitted. Also, we are interested here only in following the remarkable spontaneous separation into two size groups. The populations in each size class are not crucial to this separation. For simplicity, we take the cavity number densities in individual size classes to be equal.

Fig. 8 shows a typical result from these calculations. After 100 dpa the initial distribution has separated into a bimodal distribution with a gap of more than 50 nm. The initial distribution at the beginning of the calculation consisted of the same number of classes of small cavities, all with initial sizes of less than 9 nm, and each class containing a different number of gas atoms, covering the approximate range 50 to 40000 gas atoms.

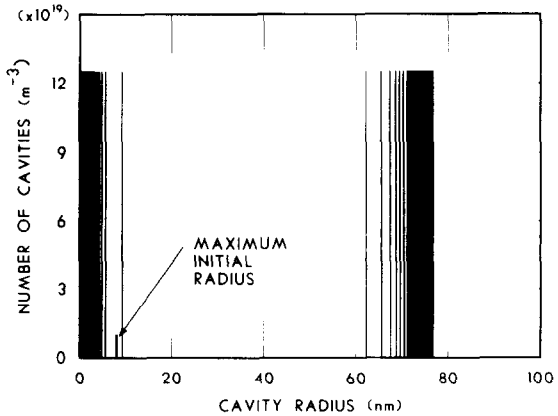

Fig. 8. Simplified theoretical calculation showing the separation into a bimodal size distribution of an initially unimodal distribution with maximum radius approximately 9 nm.

During irradiation gas was generated at a rate of 0.4 appm/dpa, typical of fast reactor irradiation.

Some of this gas was allowed to be absorbed into cavities. The instantaneous fraction of absorbed gas into each cavity size class was partitioned according to the sink strength of cavities in that size class relative to the total sink strength. The total sink strength includes the sink strengths of all other sinks. Here we take dislocations as the only other sink type. Thus the fractional absorption rate of helium in a cavity class m is given by

$$f_{\mathrm{He}}^{m} = \frac{S_{\mathrm{i}}^{\mathrm{c}m}}{\sum_{m} S_{\mathrm{i}}^{\mathrm{c}m} + S_{\mathrm{i}}^{\mathrm{d}}} . \tag{34}$$

The summation is over all cavity size classes. The symbols $S_{\mathrm{i}}^{\mathrm{c}}$ and $S_{\mathrm{i}}^{\mathrm{d}}$ are those defined earlier for the sink strengths of cavities and dislocations for self-interstitials. Thus we have assumed that the helium partitioning ratios are identical to the self-interstitial partitioning ratios.

The initial structure of the distribution was such that some cavities followed trajectory type III of figs. 1 and 3, while others followed trajectory type I. That is, some cavities contained enough gas initially to grow continually by bias driven growth while others contained only enough to grow to their individual $r_{\mathrm{c}}^{\mathrm{c}}(n_{\mathrm{g}})$. The cavities at the very largest sizes in fig. 8 exhibited behavior type III while those still in the smaller group of the bimodal exhibited behavior type I. During the irradiation, however, some of the cavities that initially contained only enough gas to exhibit behavior type I gradually accumulated enough gas to exceed n_{g}^{*}; these cavities then grew by bias-driven growth. The smallest cavities in the large size group of the bimodal distribution of fig. 8 exhibited this behavior. The gas content of the size class at the lowest size in the large group moved past n_{g}^{*} only after about 5 dpa. Interestingly, the radius of the class at the largest size in the small group also began to increase rapidly between 3 and 10 dpa. However, the increasing sink strength in the system due to cavity growth continually increased n_{g}^{*} and $r_{\mathrm{c}}^{\mathrm{c}*}$ so that this class eventually got left behind and never was able to exceed the then current $r_{\mathrm{c}}^{\mathrm{c}*}$.

Gas partitioning is crucial to the precise form of the results. Some of the earlier work had assumed that all generated gas accumulated in the cavities [5,11], although early calculations of Odette and Langley [10] included gas partitioning. Since gas accumulation takes place by diffusional processes, it is likely that gas accumulates at all sinks. To a first approximation these sink strengths may be assumed to be similar to point defect sink strengths. This generally results in less gas accumulation in the cavities. However, when gas is absorbed at dislocations it may detrap thermally or by irradiation re-solution, or with higher probability ultimately end up in small gas-vacancy clusters formed at the dislocations. These, of course, if they achieve large enough size, will need to be incorporated into the cavity size distribution. The crucial importance of gas partitioning has been emphasized in recent papers [19,29]. Greater differences in gas accumulation rates at cavities potentially can be achieved by partitioning versus not partitioning, or by partitioning using different models, than by the large differences in gas production rates in fission reactors and fusion reactors under a given partitioning model.

4. Dose dependence of swelling and the effects of helium

The dose dependence of swelling may be thought of as comprised of two stages: (1) the dose interval to the onset of bias-driven swelling and (2) the kinetics of cavity growth and further cavity nucleation. Helium may have strong effects on both these aspects.

4.1. Dose interval to the onset of bias-driven swelling

This interval is determined by the time under prevailing conditions to build up a significant number of three-dimensional vacancy aggregates capable of bias-driven growth. This interval may be somewhat arbitrary. For example, if transmission electron microscopy is used to detect cavities, the reportable onset is determined by the formation of cavities of sizes above the microscope resolution limit and of numbers sufficient to be detectable. The onset of bias-driven swelling may also occur at sizes well above the resolution limit, for high temperatures or low dose rates.

What determines the period to the onset of bias-driven swelling? This question can be answered by reference to the previous section. There we find two conditions. First the bias, $(Z_{\mathrm{i}}^{\mathrm{d}} Z_{\mathrm{v}}^{\mathrm{c}} - Z_{\mathrm{v}}^{\mathrm{d}} Z_{\mathrm{i}}^{\mathrm{c}})$, must be positive. Second, the cavities must achieve the critical radius or critical number of gas atoms for bias driven growth. From fig. 2 we see that at low temperatures and/or high dose rates the critical radius is very small. Therefore, provided the bias is positive, the formation of nearly any three-dimensional vacancy cluster will constitute the production of a cavity in bias driven growth. If the bias is not positive then bias driven growth is not possible. Since solute segregation may affect the capture efficiencies [35], it may be necessary to wait until solute segregation changes the Z's sufficiently. At higher temperatures the critical radius may

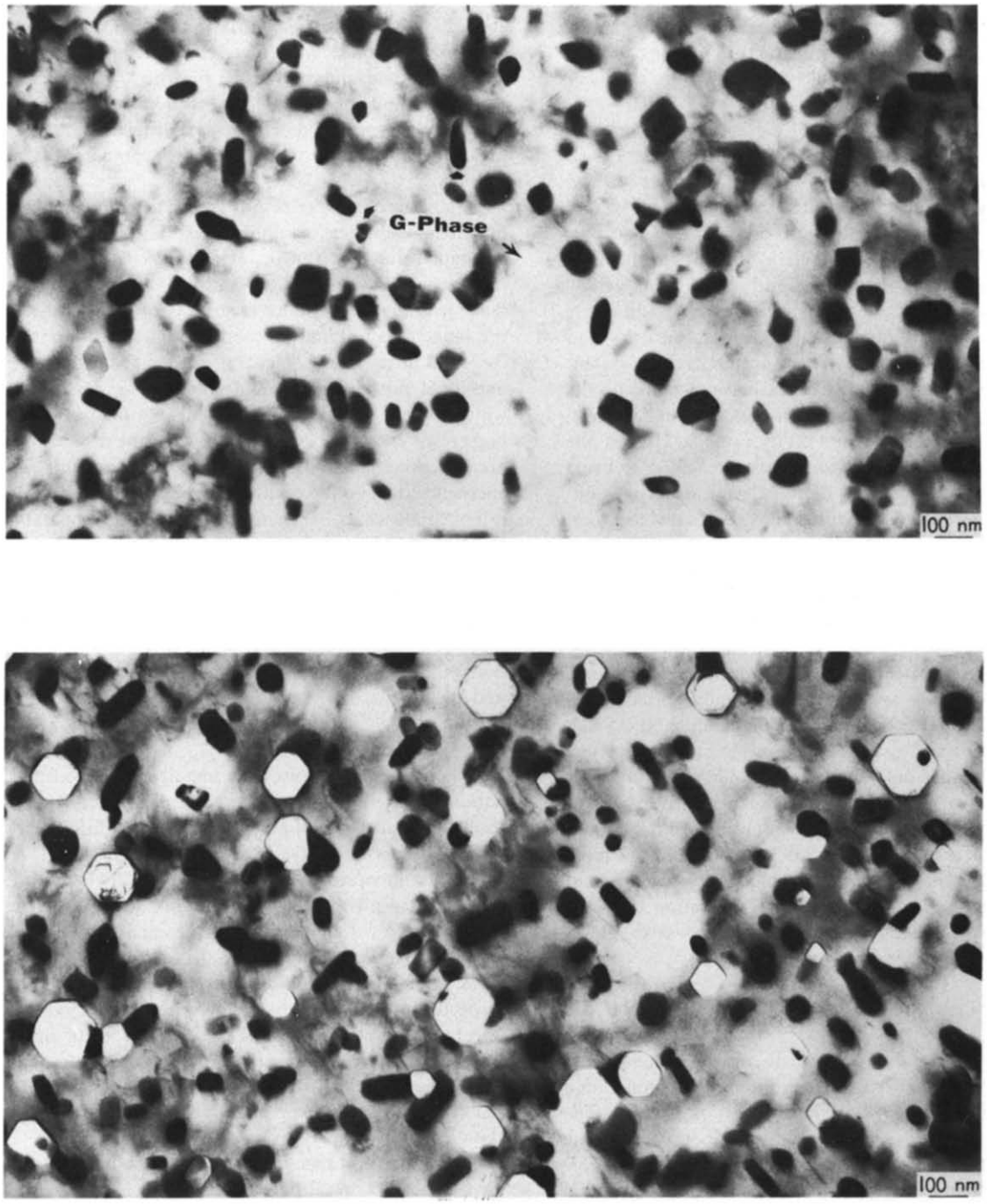

Fig. 9. Microstructure of Ti-modified type 316 stainless steel irradiated with nickel ions to 100 dpa at 675°C. Upper micrograph is the result for irradiation with nickel ions only and lower micrograph is the result for simultaneous irradiation with nickel ions and injection with helium at a rate of 0.4 appm/dpa. From ref. 36 (see also refs. 42 and 47 for supporting results).

be quite large even with a large bias. As shown in the previous section, however, this can be reduced essentially to zero if there are sufficient numbers of gas atoms contained in the cavity. Thus gas pressure may be crucial to bringing about bias-driven swelling at higher temperatures.

Fig. 9 shows an example of the microstructures produced in a titanium-modified type 316 stainless steel irradiated with Ni-ions to a dose of 100 dpa at 675°C with no helium injection, and with simultaneous helium injection at a rate of 0.4 appm/dpa [36] (see also refs. 42 and 47 for supporting results). Without gas the alloy shows pronounced segregation and precipitation behavior. The solid solution is transformed into a multi-phase system containing large blocky G-phase particles and some finer MC particles. There are no cavities present With gas injection the same phase decomposition occurs and the precipitate microstructures are similar. Here, however, there is significant cavity swelling. Helium, the only difference in the irradiations, is essential to bring about swelling. An even more extreme result was obtained in a similar Ti-modified alloy designated as LS1A, irradiated with Ni ions with no gas injection. The dose achieved was 600 dpa and there was no cavity swelling [37]; the same material irradiated to 100 dpa with simultaneous helium injection exhibited significant swelling.

Theoretical calculations on systems containing only dislocations and cavities lead to similar results with respect to the effect of helium. For example, in calculations leading to fig. 8 described in the previous section, it is found that only those cavities initially containing more than n_g^* gas atoms achieved bias driven growth immediately. Other cavities did not grow past r_c^{c*} until in the course of the irradiation they accumulated more than n_g^* gas atoms. When not enough gas was present initially and simultaneous helium generation was suppressed, no cavities grew and the swelling was absent, as also observed in the experiments.

4.2. Cavity growth kinetics

In a systematic analysis of the dose dependence of cavity swelling under many conditions [20] it was found that a wide range of dose dependence is possible. The result is dictated by the relative importance of the competing modes of point defect loss. In a simple system where losses to cavities, dislocations, and mutual recombination are the primary fates of point defects, the dose exponents of swelling are determined mainly by five considerations: (1) the relative importance of sinks versus mutual recombination, (2) which of the sinks is the dominant one, (3) the dose dependence of the dislocation density, (4) the mode of point defect absorption at the cavity matrix interface, i.e., whether diffusion controlled or surface reaction controlled, and (5) the dose dependence of the bias. In limiting cases where one mode of point defect loss dominates, and for analytically represented behaviors of dislocation density with dose, the dose exponents can be worked out analytically.

A table giving these results for systematic combinations of possibilities, assuming the bias has achieved a constant value, is given in ref. 20. Except for unusual cases where the dislocation density is decreasing with dose, it is found that dose exponents of swelling lie in the range $\frac{3}{5}$ to 3. Limiting cases as well as non-limiting cases fall in this range. Generally, when the dislocation density is not changing rapidly with dose, a situation which is very common after a relatively low dose, the higher exponents are encountered when the dislocations are the dominant sink and the lower exponents are encountered when the cavities are the dominant sink. In intermediate cases, when the sinks are of comparable strength, the dose exponent of swelling is predicted to be near unity.

In that analysis the parameters we define as q and Q are prominent.

$$q = 4RG/K_v K_i, \tag{35}$$

and

$$Q_{i,v} = Z_{i,v}^d L/4\pi r_c N_c Z_{i,v}^c. \tag{36}$$

The parameter q measures the importance of recombination relative to loss to sinks. The parameter Q measures the importance of point defect loss to dislocations relative to loss to cavities.

Fig. 10 illustrates the results schematically for $q \ll 1$. In traversing all three regimes of sink strength, where dislocations are dominant ($Q \gg 1$), comparable ($Q \sim 1$), and minor ($Q \ll 1$) compared to the cavity sink strength, the swelling versus dose dependence is predicted to be respectively greater than linear, linear, and less than linear with respect to dose. This is shown in the upper part of the figure. However, the ratios of sink strengths in real materials are often such that all three regimes are not traversed in an experiment. These possibilities are shown in the lower part of fig. 10. For example, in stainless steels irradiated in fast reactors, all the data we have examined reveal the material to be in the regimes ranging from $Q \gg 1$ to $Q \gtrsim 1$, even at the highest doses. Thus we expect greater than linear to roughly linear dose dependencies. This expectation is indeed confirmed in an extensive body of data. In pure materials

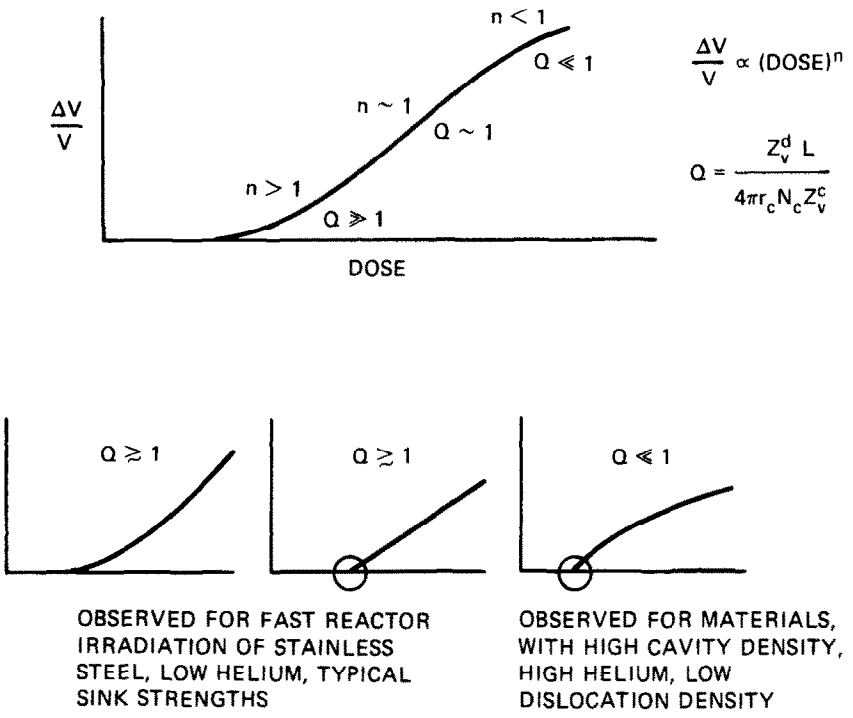

Fig. 10. Schematic summary of theoretically predicted dose dependencies of swelling.

such as nickel and aluminum, on the other hand, the dislocation density is often low, so that the regime $Q \ll 1$ is observed. There we expect the dose exponent to be less than linear. This again has been confirmed [38]. In an irradiation of molybdenum, the cavity density is very high leading to $Q \ll 1$. Again the less than linear dose exponent of swelling has been observed [39].

How does helium enter this picture? Helium is known to affect the cavity density and, to a lesser extent, the dislocation density [40]. The degree depends upon how much helium is involved and on how it is introduced. Fig. 11 from the work of Packan and Farrell [41] shows three examples of observed swelling versus dose in a high purity stainless steel (Fe–17Cr–16.7Ni–2.5Mo), ion irradiated at doses up to 70 dpa. The three curves represent Ni ion irradiation, Ni ion irradiation with simultaneous helium injection at a rate of 20 appm/dpa and Ni ion irradiation with helium preinjected to give a ratio of 20 appm/dpa for each dose point. The value of Q corresponding to the 70 dpa points is written beside each curve. * For $Q \sim 1$ the curves are linear as expected from the theory. For $Q < 1$ in the case of the preinjected material, the curve bends over and shows a less than linear dose dependence as expected. However, the effect is even more pronounced than expected. There may be other contributions to this behavior from possible effects of helium upon the bias [16], and from the appearance of a second class of small cavities leading to a bimodal cavity size distribution.

The effects of this second class of cavities on the swelling behavior can be described by an extension of the analysis of ref. 20. These cavities, as long as they remain below the critical radius, do not contribute to the increase in swelling directly, except as their density increases. However, they do act as sinks for point defects and may thus affect swelling indirectly. Of course all point defects absorbed at these cavities recombine, except as further helium is accumulated some of the vacancies escape recombination and are accommodated in the cavities. In the theory, mutual recombination and absorption at sinks are accounted separately, although

* The quantities Z_v^d and Z_v^c, the sink capture efficiencies, in eq. (36), are not known precisely. On the assumption that their ratio is near unity the quantity $Q' = L/(4\pi r_c N_c)$ is approximately equal to Q. It is the values of Q' which are shown in fig. 11.

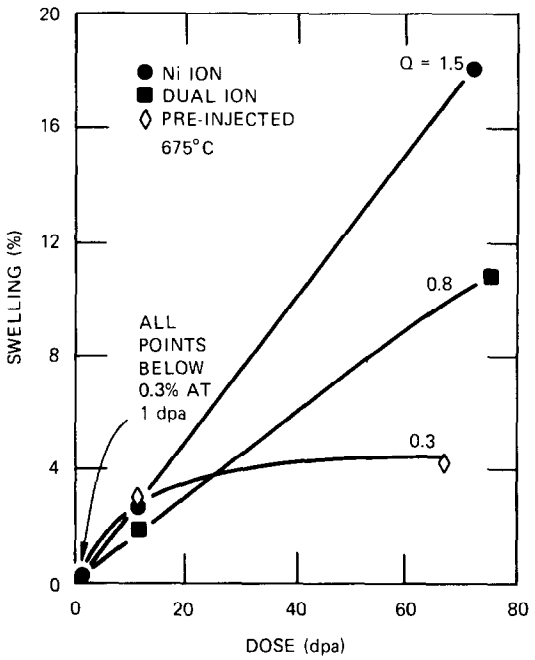

Fig. 11. Observed dose dependence of swelling in a "pure" stainless steel. The irradiations covered the range up to 70 dpa and the irradiation temperature was 625°C. The behavior with no helium, with simultaneous helium injection and with helium preinjection is shown. From ref. 41.

of course most of what is absorbed at sinks recombines there. The small stable cavities may therefore increase the overall fraction of point defects recombining and affect the magnitude of swelling by changing the losses to dislocations and growing cavities. The dose exponent of swelling may also be affected.

The more precise statement of cavity growth is mathematical and can be obtained by substituting eqs. (8) and (9) into (10), for simplicity neglecting thermal vacancy emission, and specializing to a three sink system – dislocations, growing cavities, and stable cavities. The result is [20]

$$\frac{dr_c}{dt} = \frac{\Omega G}{r_c}\Big\{ L\left(Z_i^d Z_v^c - Z_i^c Z_v^d\right) + 4\pi r_s N_s \left(Z_i^s Z_v^c - Z_v^s Z_j^c\right)\Big\} \times \Big\{\left(Z_v^d L + 4\pi r_c N_c Z_v^c + 4\pi r_s Z_v^s N_s\right) \times \left(Z_i^d L + 4\pi r_c Z_i^c N_c + 4\pi r_s Z_i^s N_s\right)\Big\}^{-1}. \quad (37)$$

The quantities with superscripts and subscripts "s" are the analogs to the quantities already defined for dislocations and cavities, where these new symbols denote the stable cavities. If we assume for simplicity that there is no capture efficiency difference between the cavities and the stable cavities then $(Z_i^s Z_v^c - Z_v^s Z_i^c) \to 0$. This simplifies eq. (37) considerably. If $4\pi r_s Z^s N_s \ll Z^d L$, $4\pi r_c Z^c N_c$ then the result reduces to that discussed above where there are no stable cavities and the results of ref. 20 and fig. 10 apply. If, however, the stable cavities are the dominant sink – the real case of interest here – we obtain

$$\frac{dr_c}{dt} = \frac{\Omega G}{r_c}\left(Z_i^d Z_v^c - Z_i^c Z_v^d\right)\frac{L}{(4\pi r_s N_s)^2 Z_i^s Z_v^s}. \quad (38)$$

Clearly $(r_s N_s)^2/L$ will have some time (dose) dependence. We approximate it over the dose interval of interest as $(r_s N_s)^2/L \propto t^h$, where h is the exponent of the dependence. For illustration, we take the bias term as constant. Integrating eq. (38) then gives $r_c \propto t^{(1-h)/2}$ or $\Delta V/V \propto t^{3(1-h)/2}$. For $h = 0$, i.e., for constant microstructure of stable cavities and dislocations, we obtain $\Delta V/V \propto t^{3/2}$, the same result as for a two sink system with dislocations dominant. On the other hand, whenever $(r_s N_s)^2/L$ is proportional to dose to a power greater than $\frac{1}{3}$, then the dose dependence of swelling becomes less than linear.

We may summarize this section by the statement that the influence of helium on the dose dependence of swelling can be significant, and that the effect is manifest through the changes in the relationships among microstructural sink strengths and among their evolution rates. There is also some evidence that helium changes the bias by changing individual sink capture efficiencies. The theoretical results are testable when microstructural parameters have been measured. The theory has proven consistent with measured dose dependences of swelling over a wide range of materials and microstructures.

5. Helium, phase instability, and swelling

The study of phase instability in alloys during irradiation is a subject of growing interest. Its understanding is less complete and quantitative than the areas of swelling discussed in earlier sections. This is at least partly because this topic has only recently become of widespread interest. The interaction of helium with phase instability is of special interest in the present paper. Several types of observations of helium effects will be reviewed and possible underlying mechanisms discussed.

5.1. Cavity formation at precipitate–matrix interfaces

A prevalent observation is that cavities nucleate at precipitate–matrix interfaces. Helium is known to be involved in the nucleation of these cavities in stainless steels. In fig. 9, for example, it is clear that the helium is responsible for the cavity nucleation at the precipitate matrix interfaces.

In other experiments using similar alloys with higher amounts of helium, it is found that the helium is responsible for nucleating cavities both at the precipitate–matrix interfaces and in the matrix. Fig. 12 shows the results of a sequenced nickel ion and helium ion injection experiment [42]. A titanium-modified type 316 stainless steel was first irradiated with nickel ions to 70 dpa (left). This resulted in the appearance of large G-phase particles but with no swelling. Next helium ions were injected to a level of 400 appm (middle). This resulted in the appearance of many small bubbles located both at the G-phase precipitate–matrix interfaces and in the matrix. After the helium injection the nickel ion irradiation was resumed for a further 20 dpa (right). This resulted in the growth of the cavities created by the helium injection. An interesting result was observed. The cavities on the precipitate matrix interfaces grew larger than the ones in the matrix. This result had been predicted theoretically [43] and the experiment was designed to test the prediction. The enhanced growth results from point defect collection on the precipitate–matrix interface and diffusion of the defects along the interface to the cavity. Point defect collection also reduces the critical radius and the critical number of gas atoms for the attached cavity, and this in turn reduces the time interval to the onset of bias-driven swelling. The above experiment was designed to separate the enhancement in growth rate in order to make a simpler quantitative comparison.

There are three mechanisms we believe to be im-

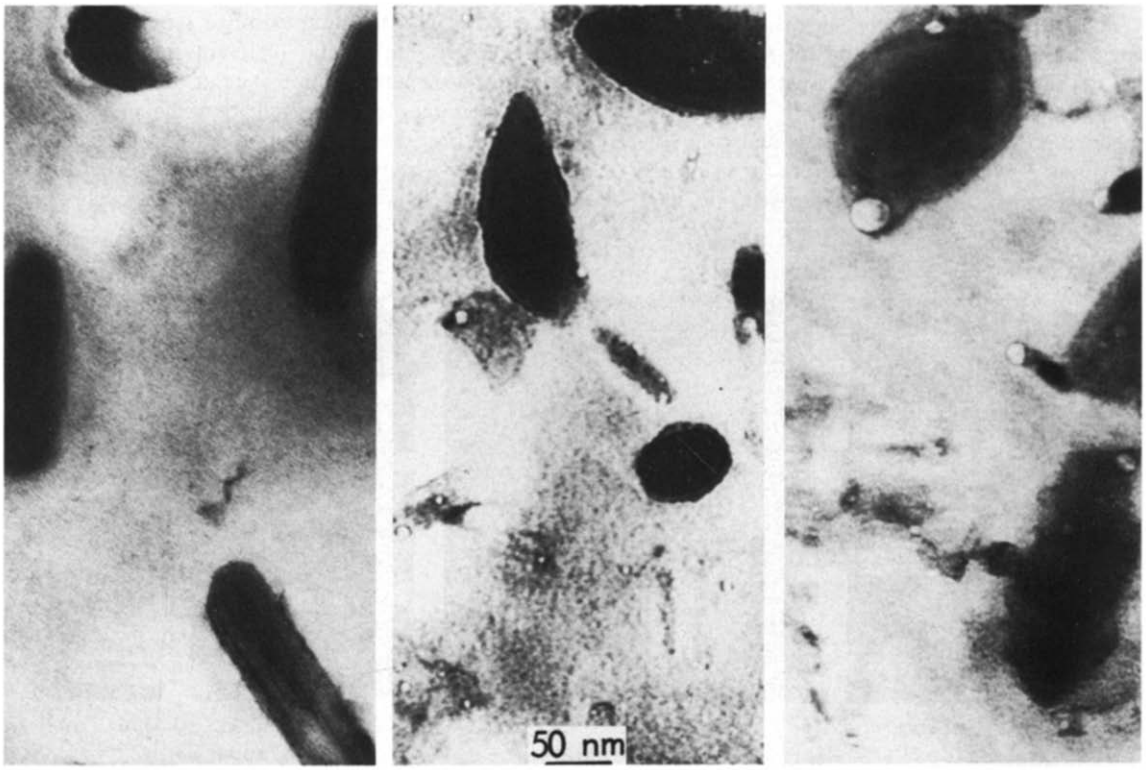

Fig. 12. Microstructures developed as 675°C in a titanium-modified type 316 stainless steel in a sequenced heavy ion and helium injection experiment. The left micrograph is after nickel ion irradiation to 70 dpa. The center micrograph shows the result after nickel ion irradiation to 70 dpa, with subsequent helium injection to a level of 400 appm. The micrograph on the right shows the results after the same treatment as the center micrograph but with an additional nickel ion irradiation of 20 dpa. From ref. 42.

portant in favoring cavity formation on interfaces as in the experimental observations cited above. These can be designated as

(1) Point defect collection,
(2) Helium trapping,
(3) Surface energy credit.

Helium trapping and accumulation at the interface has been proposed several years ago (see for example ref. 44). Recently, experimental evidence for helium accumulation at interfaces has become very strong. Work of Lee et al. [42] using high resolution electron microscopy has revealed very small cavities at low doses on the precipitate–matrix interfaces in ion irradiation experiments. Such cavities were not seen in the absence of injected helium. Large fractions of the precipitate–matrix interfaces were covered with the small cavities, indicating that the helium was accumulating locally at many regions of the interface. Since helium lowers the critical cavity radius, as shown in §3, this gives in principle a mechanism for the initiation of swelling at precipitate–matrix interfaces.

The interfacial energy credit is a widely appreciated cause for the preferred nucleation of cavities on interphase interfaces [45]. In a single phase material the formation of a cavity requires work to create the surface. In a two phase material, however, work has already been expended to create the precipitate–matrix interface. In creating a cavity at this interface, a region of the precipitate–matrix interface is destroyed, yielding its energy to help in creating the cavity–precipitate and cavity–matrix interface. Recently, Stoller and Odette [17] have included this mechanism in a rate theory model for cavity swelling.

5.2. *Helium-induced changes in phase stability*

Recent experiments have revealed that helium may influence the type and distribution of precipitates that occur during irradiation [46–49]. Three types of observations may be noted, although these might be viewed as differences of degree in the same phenomena. Helium may:

(1) produce an overall suppression of irradiation-related precipitation and swelling;
(2) arrest, delay, or change the normal sequence of phase transformations during irradiation:
(3) change the mixture of precipitate phases present after a given dose.

Fig. 13 is a set of micrographs representing nickel ion irradiations at 625°C to the same dose of 70 dpa, but each with different modes of helium injection [46]. The material is a titanium-modified type 316 stainless steel. The left micrograph represents irradiation with simultaneous helium injection at a rate of 0.2 appm/dpa. At the beginning of the irradiation the material was essentially precipitate-free on the scale of the micrograph. After irradiation, extensive transformation to G-phase can be seen. Significant swelling occurs. The

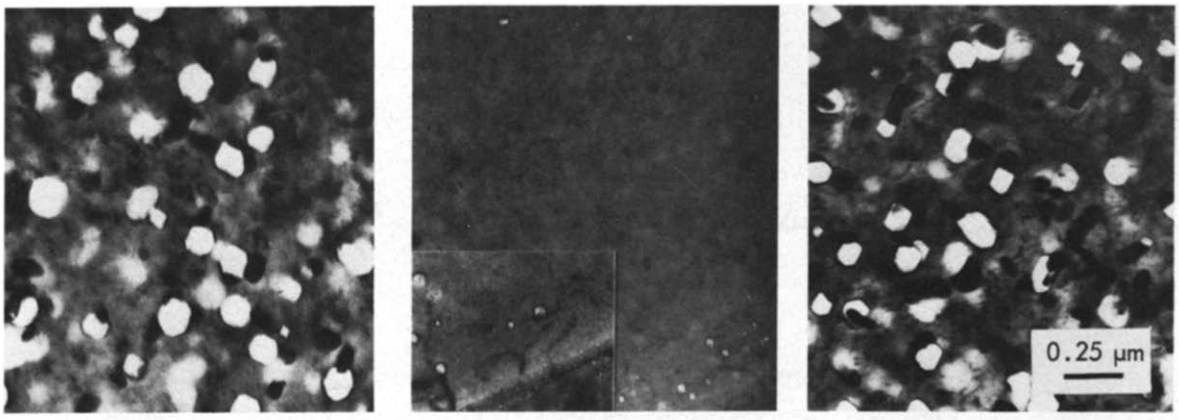

Fig. 13. Microstructures developed at 625°C in a titanium-modified type 316 stainless steel. The left micrograph represents nickel ion irradiation to 70 dpa with simultaneous helium injection at a rate of 0.2 appm/dpa. The center micrograph is to the same dose but with 14 appm helium preinjected. The right micrograph is again to the same dose. Here the nickel ion irradiation was interrupted at 10 dpa, whereupon 14 appm helium was injected and the nickel ion irradiation was then continued. From ref. 46.

middle micrograph represents the same dose but with 14 appm He injected prior to the irradiation. The difference is dramatic. The extensive transformation to G-phase usually observed is absent. Swelling is negligible. The right micrograph also represents heavy-ion irradiation to the same dose. The irradiation sequence was altered, however. Nickel ion irradiation was interrupted at 10 dpa. At this point 14 appm He was injected. Following this the heavy ion irradiation was continued to a total dose of 70 dpa. Here, however, extensive transformation to G-phase again occurred, with significant accompanying swelling. Many of the large cavities are attached to precipitates.

Fig. 14 shows a similar material (a titanium-modified type 316 stainless steel) irradiated with nickel ions with and without simultaneous helium injection [47]. The material was initially in a cold worked state in this case, however. On the top is the microstructure after 5 dpa with helium injection at 0.4 appm/dpa. Extensive fine MC precipitation on the dislocation network is evident. The microstructure at 5 dpa of uninjected and simultaneously helium injected specimens at 20 appm/dpa are essentially identical to this. In the center is a micrograph of the specimen irradiated to a dose of 70 dpa. The MC phase present at 5 dpa has almost disappeared and extensive transformation to much larger G-phase particles has occurred. Swelling is also observed in the simultaneously injected material, mainly caused by cavities attached to G-phase particles. The situation is, however, quite different for the material injected at a rate of 20 appm/dpa and irradiated to a dose of 70 dpa, as shown on the bottom. Even at 70 dpa the microstructure still contains a very high density of fine MC precipitates and no G-phase particles, except in a few isolated recovered areas. Swelling is again negligible. Each MC particle, however, appears to have a very small cavity attached to it. This experiment clearly shows that a high helium injection rate, typical of that expected in a fusion reactor first wall, has drastically changed the "normal" sequence of phase transformations.

Evidence for helium effects on phase stability is also available for neutron irradiated materials [48]. In these experiments, large differences in helium generation have been achieved by using the EBR-II, a high flux fast spectrum reactor, and the HFIR, a high flux mixed fast and thermal spectrum reactor. In the EBR-II the helium generation rate is low, in the range of tenths of appm/dpa. In the HFIR, a water moderated mixed spectrum reactor, the thermal component of the spectrum produces large amounts of helium by a two step transmutation reaction of nickel, accumulating up to thousands of appm He in irradiations of stainless steel type alloys to doses of the order of 50 dpa. The accumulation rate is greater than linear but less than quadratic with dose.

Fig. 15 shows histograms of the volume content of precipitates in a non-titanium modified heat of type 316 stainless steel [49] (ref. 48 contains data shown in the figure). Where the doses are comparable, e.g., at 69 dpa in EBR-II and 61 dpa in HFIR it is clear that there are differences in the mixtures of precipitates. In detail there are also differences in the dispersions and associations of cavities with other microstructural features. Fig. 15 shows, however, that even the precipitate volume fractions are quite different. The HFIR material contains no reported G-phase or γ' phase, while the EBR-II material contains significant proportions of both. The HFIR material contains significantly more Laves phase than does the EBR-II material. The composition of the Laves phase is also different. In the HFIR material the nickel content of the Laves phase is approximately 12%, while in the EBR-II, the nickel content ranges from approximately 20 to 40% between the doses of 36 and 69 dpa. These changes in composition and phase mixture have been interpreted as effects of helium on solute segregation [48].

In view of the large differences in microstructure produced by helium in the single variable ion irradiation experiments, it is considered likely that the above differences mainly are due to differences in helium generation rate in the two reactors. Here, however, it should be pointed out that the situation is less clear cut than in the ion irradiation cases because of the differences in neutron spectra and reactor environment. Other interpretations have also been proposed. Brager and Garner [50] interpret differences as due to production of V and burnout of Mn in HFIR. It is highly desirable that single variable neutron irradiation experiments be designed to isolate the effect of helium and remove complicating factors.

Helium effects on phase stability are obviously complex. The materials on which the experiments were performed are similar to commercial stainless steels. Quantitative theoretical modeling of the same level as discussed in earlier sections is not yet available. However, mechanisms can be suggested which may clarify these observations.

When an irradiation is initiated, interstitial dislocations loops nucleate rapidly. The slower vacancies eventually diffuse to the loops and annihilate many of them. The remaining loops serve as sites for solute segregation and eventually G-phase precipitates nucleate there. Introducing helium alters this picture. The vacancies which

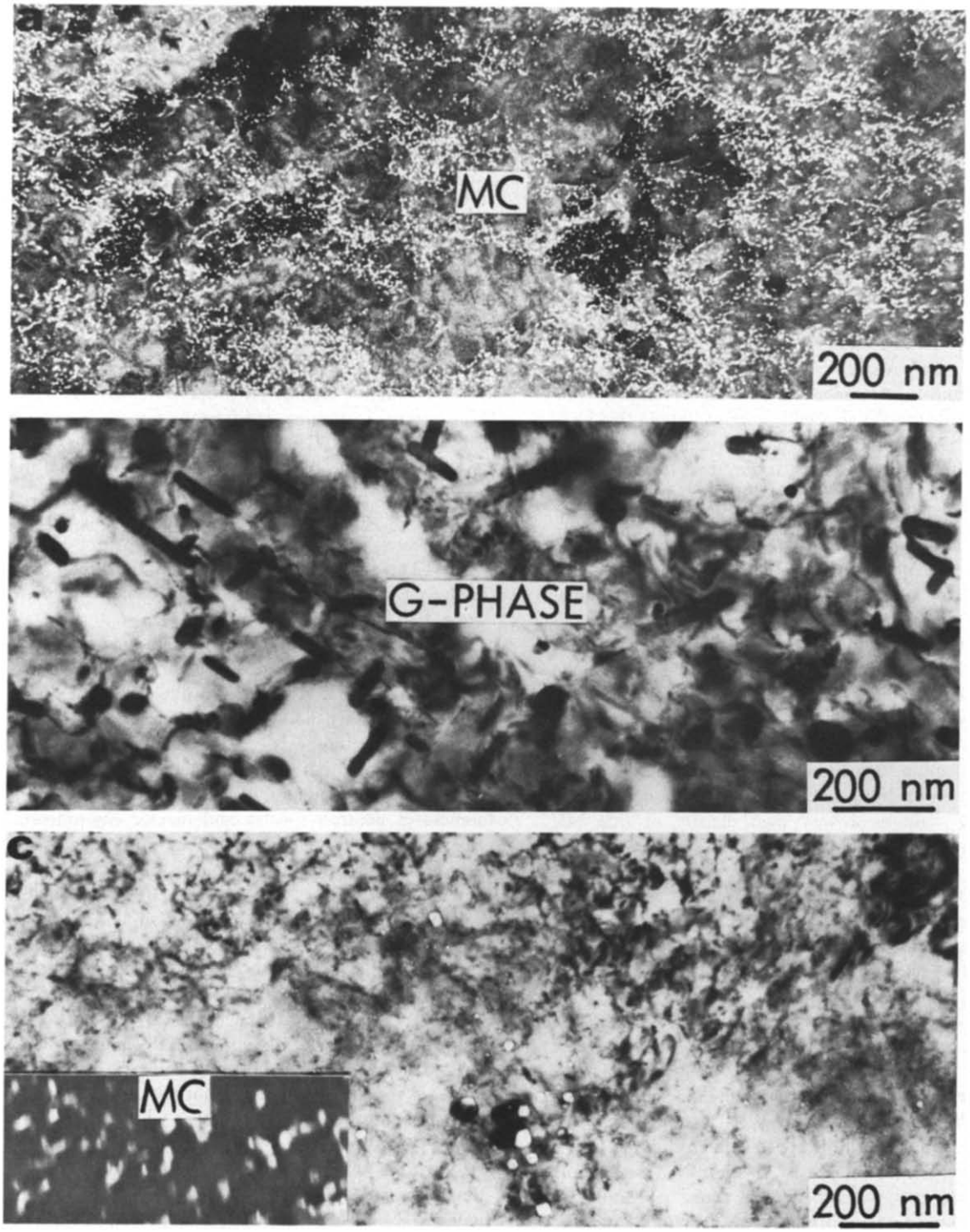

Fig. 14. Microstructures developed at 675°C in 20% cold worked titanium modified type 316 stainless steel. On the top is the result of nickel ion irradiation to 5 dpa with 0.4 appm He/dpa. Microstructures for nickel ion irradiation and for simultaneous injection at 20 appm/dpa are virtually identical. In the center is the result at 70 dpa with simultaneous helium injection at 0.4 appm/dpa. On the bottom is the result at 70 dpa with simultaneous helium injection at 20 appm/dpa. From ref. 47.

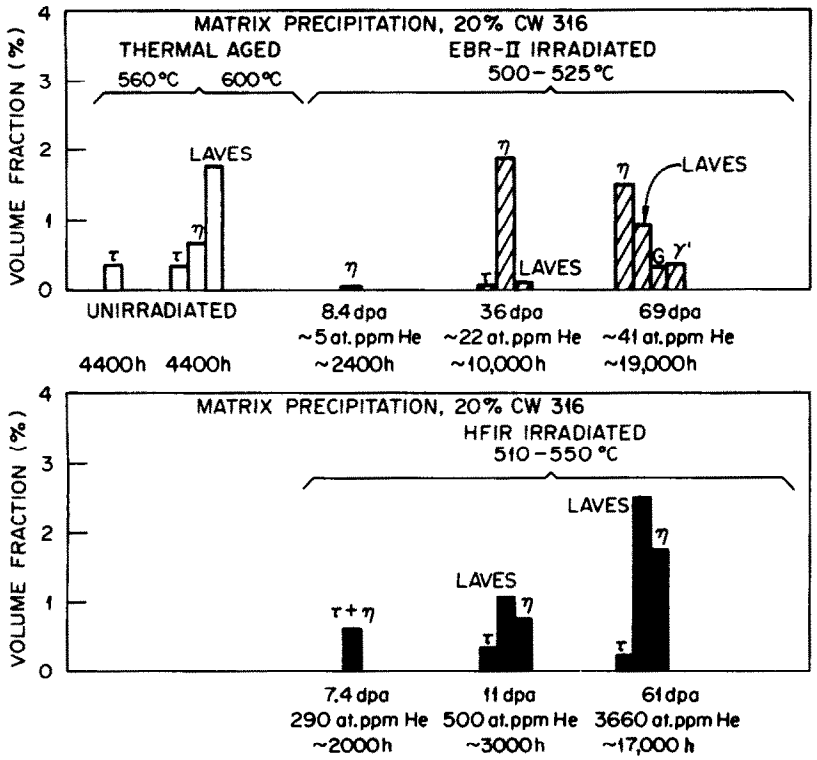

Fig. 15. Histograms showing the volume fractions of important precipitates after irradiations in EBR-II and HFIR to several doses. From ref. 49 (ref. 48 contains data shown in the figure).

would otherwise diffuse to loops are immobilized in helium–vacancy clusters. This produces more sinks for point defects – the retained loops and the helium–vacancy clusters or cavities. This larger number of sinks increases the number of sites for solute segregation. However, the number of solute atoms per unit volume is fixed so that the enrichment at each site is reduced. With enough reduction the enrichment passes below the solubility limit for precipitation of the phase that would otherwise occur. This seems to explain the overall suppression of phase instability by helium. It also helps explain the increased stability of MC phase in the presence of helium. In this case, a further stabilizing mechanism appears to be the attachment of cavities to MC precipitates. MC is a strongly misfitting phase. A cavity relaxes the strain and reduces the energy of the system. Thus the overall effects of helium on phase stability though they are complex, again appear to depend at least in part on helium trapping of vacancies.

6. Summary

In this paper we have reviewed and further developed aspects of the theory underlying several mechanisms by which helium may influence radiation effects in metals and alloys. Helium produces major influences on the evolution of mirostructure and microcomposition during irradiation. The many effects of helium considered here can be attributed to three main modes of action, which are of course not independent. These are designated as changes in the critical cavity radius for bias-driven growth, changes in the overall point defect sink strength and changes in radiation induced solute segregation and precipitation. In the first two areas the discussion is developed in terms of quantitative theoretical analysis. In the third area the theoretical description of the precipitate point defect collector mechanism, relating enhanced cavity growth to precipitation, has been developed recently and is cited as an example.

Other aspects of changes in microcomposition by helium are discussed more qualitatively.

6.1. Critical cavity radius

The critical radius for bias-driven growth arises from a competition between cavity growth induced by biased radiation induced point defect fluxes and cavity shrinkage induced by thermal vacancy emission. In the past literature the critical cavity radius has been the subject of a significant amount of attention and aspects of its behavior and parametric dependence have been worked out.

In the present paper we review and further develop the concept. As examples, both the ideal gas and the Van der Waals gas are considered. A set of analytical results is derived for each. Expressions for the gas free critical radius, r_c^{c0}, are given. As gas is added the critical radius is reduced. There is a maximum number of gas atoms that can be added, n^*_g which results in a minimum finite critical radius r_c^{c*}. If any more gas is added, the critical radius effectively disappears, meaning that there is then no barrier to cavity nucleation. Remarkably simple results are obtained from this analysis. The first is that $r_c^{c*}/r_c^{c0} = 2/3$. Another very important result is that $P_g^*(r_c^{c*})/P_g^{eq}(r_c^{c*}) = 1/3$. This means that when a cavity is at the minimum critical radius, r_c^{c*}, the gas pressurization necessary to remove the nucleation barrier is only one-third of the gas pressurization required for an equilibrium bubble. The results above are for the ideal gas. Somewhat more complicated results are also available for the Van der Waals gas. Nevertheless, these can also be expressed analytically. For large r_c^{c*}, the two gas laws lead to similar results. The small cavities below critical radius are in principle not equilibrium bubbles. The critical radii derived in cavity growth and in cavity nucleation theory are equivalent.

The fact that r_c^c is reduced by gas gives rise to the theoretical prediction that swelling will take place at higher temperatures with gas. This is commonly observed experimentally. It also follows that gas reduces incubation time and may in fact make swelling possible at high temperature. In general there are two physical solutions of the cavity growth rate equation giving zero growth rate. One is the critical cavity radius r_c^c, the other is a stable cavity radius r_c^s. The existence of r_c^s and r_c^c give rise to the theoretical expectation of bimodal cavity size distribution when gas is present. The cavities in the smaller group of the bimodal will remain stationary at their r_c^s corresponding to each n_g. If they can achieve r_c^c by point defect flux fluctuation or by variations in irradiation conditions, or can absorb more than n_g^* gas atoms regardless of their size, they will enter the larger group of the bimodal distribution and grow indefinitely by bias driven growth. Bimodal cavity size distributions are commonly observed in irradiated materials containing helium. In numerical example calculations unimodal cavity size distributions spontaneously break up into bimodal distributions.

6.2. Dose dependence of swelling

The dose dependence of swelling may be thought of as comprised of two physical regimes. The first is the dose interval to the onset of bias driven swelling while the second is the behavior during bias driven swelling. The onset is determined strongly by gas content and by the influence of gas on the critical cavity radius.

One of the important contributions of the theory of cavity swelling has been to provide a comprehensive picture of the cavity growth kinetics regime. Two important factors in the theory for a simple two sink system are q, the ratio of loss of point defects by mutual recombination to loss to sinks, and Q, the ratio of loss of point defects to cavities to loss to dislocations. When the dislocation density is not changing rapidly with dose it is found that the dose exponent of swelling is greater than unity when $Q > 1$. When $Q \sim 1$ the dose exponent of swelling is near unity and the magnitude of the swelling rate is maximum. When $Q < 1$, corresponding to cavities being the dominant sink, the dose exponent of swelling is less than unity and the magnitude of the swelling rate is reduced. The dose exponents possible in physically reasonable cases span the range from $\frac{3}{5}$ to 3.

Helium enters this picture in two ways. It increases the concentrations of growing cavities, thereby moving the system from higher to lower Q values. In extreme cases this leads to less than linear dose dependence of swelling. In addition it may introduce a third sink into the system – the small stable cavities below the critical radius. These small cavities also absorb point defects which ultimately recombine. When the sink strength of these cavities dominate, the kinetics of swelling is altered from that in the two sink system. The precise behavior depends on how the ratio of the stable cavity sink strength to dislocation sink strength varies with dose. Experimentally observed dose dependences of swelling with and without high helium contents have been found to be consistent with this picture.

6.3. Helium, phase stability, and swelling

There is strong experimental evidence for helium interaction with solute segregation and phase stability.

On the one hand this interaction leads to changes in swelling. Helium nucleates cavities at precipitate–matrix interfaces. Once nucleated, these cavities grow more rapidly than cavities in the matrix. It has been found theoretically and experimentally that this enhanced growth results from point defect collection at the precipitate–matrix interface and diffusion to the attached cavity. Helium also affects the segregation and precipitation processes themselves. Helium may suppress overall precipitation; it may delay or change the sequence of transformations normally observed under irradiation in the absence of helium; or it may change the mixture of types of precipitate or the composition of given precipitates. All these effects have been observed experimentally.

The explanation we have proposed for the changes in solute segregation and precipitation induced by helium depends on the changes in overall sink density, particularly that of cavities, induced by the helium. A high cavity density lowers the average point defect concentrations and provides more sites for solute segregation and precipitation. The former effect retards the kinetics of solute segregation processes which depend upon point defect fluxes while the latter effect requires that a fixed number of segregating solute atoms is diluted among more sites. Precipitate compositions and dispersions are thus altered. The possibility of certain precipitation reactions may be eliminated entirely when the dilution ensures that the solubility limit is not exceeded at a given solute segregation site.

Acknowledgment

We are grateful for helpful discussions and comments from colleagues, particularly Drs K. Farrell, E.H. Lee, and P.J. Maziasz, of Oak Ridge National Laboratory, Professor W.G. Wolfer of the University of Wisconsin, and Professor G.R. Odette of the University of California at Santa Barbara. We thank Judy Young for her devoted efforts in preparing the manuscript.

Appendix A

The derivations of §3 are in the formalism of cavity growth theory. The critical radius is defined by the condition of zero net volume influx to the cavity. In cavity nucleation theory, a prominent result is also the existence of a critical radius [7,23,24]. There it is determined by the condition that the kinetically defined analog to the free energy be at its maximum. This is the nucleation barrier and any fluctuation resulting in a radius larger than this critical radius is said to nucleate a cavity. Thereafter, by the cavity continuing to increase in size, the analog to the free energy is continually lowered and thus growth is favored. The critical radii obtained from cavity growth theory and from cavity nucleation theory are equivalent. This is necessary result, and for convenience we summarize a procedure to show that the peak in the nucleation curve corresponds to the vanishing of the net point defect flux.

To accomplish this we employ the formulation of nucleation theory of Mansur and Wolfer [51], which follows the work referred to above but uses a formalism compatible with §3. Here it is more convenient, however, to describe the cavity size by the number of vacancies rather than by the radius. The change in the number of vacancy clusters containing n vacancies with respect to time, $\partial q(n)/\partial t$, is the difference between the number arriving per unit time from size $n-1$, $M(n-1)$, and the number leaving per unit time to size $n+1$, $M(n)$, where

$$M(n) = \beta_v(n)q(n) - [\beta_i(n+1) + \alpha_v(n+1)]q(n+1), \tag{A1}$$

and is given by

$$\begin{aligned}\partial q(n)/\partial t &= M(n-1) - M(n) \\ &= [\beta_i(n+1) + \alpha_v(n+1)]q(n+1) \\ &\quad - [\beta_v(n) + \beta_i(n) + \alpha_v(n)]q(n) \\ &\quad + \beta_v(n-1)q(n-1),\end{aligned} \tag{A2}$$

where $\beta_{v,i}(n)$ is the capture rate of vacancies, interstitials by a vacancy cluster containing n vacancies, and $\alpha_v(n)$ is the emission rate of vacancies from a vacancy cluster containing n vacancies. Here we make the correspondence $n \to r_c$. Eq. (A2) has two steady-state solutions corresponding to $\partial q(n)/\partial t = 0$. If $M(n-1) = M(n) = 0$ there is no net flux of vacancy clusters to larger sizes. This corresponds to the constrained distribution [45]. We denote the number of vacancy clusters of size n for this constrained distribution as $q^0(n)$. Eq. (A1) gives

$$\beta_v(n)q^0(n) = [\beta_i(n+1) + \alpha_v(n+1)]q^0(n+1). \tag{A3}$$

Employing this as a recursion relation we obtain

$$q^0(n) = \sum_{l=1}^{n-1} \frac{\beta_v(l)q^0(1)}{\beta_i(l+1) + \alpha_v(l+1)}. \tag{A4}$$

This may be written as

$$q^0(n) = q^0(1)\exp[-\Delta G(n)/kT], \tag{A5}$$

with the definition

$$\Delta G(n) = -kT \sum_{l=1}^{n-1} \ln \frac{\beta_v(l)}{\beta_i(l+1) + \alpha_v(l+1)}, \qquad \text{(A6)}$$

where $\Delta G(n)$ is the kinetic analog of the free energy of formation of a cluster containing n vacancies. In these equations $\alpha_v(n)$ and $\beta_v(n)$ can be expressed in terms of point defect concentrations as follows

$$\alpha_v(n) = 4\pi\Omega^{1/3} n^{1/3} Z_v^c(n) D_v C_v^c(n) / (4\pi/3)^{1/3}. \qquad \text{(A7)}$$

where $C^e(n)$ is given by eq. (11), where $r_c = (3\Omega n/4\pi)^{1/3}$. We also have

$$\beta_{i,v}(n) = 4\pi\Omega^{1/3} n^{1/3} Z_{i,v}^c(n) D_{i,v} C_{i,v} / (4\pi/3)^{1/3}, \qquad \text{(A8)}$$

where C_i and C_v are the point defect concentrations given by eqs. (8) and (9).

The second steady-state solution to eq. (A2) is that for which $M(n) = M(n-1) = \ldots \equiv M$, where M is defined as the steady-state nucleation rate. Using eqs. (A1) and (A3), we find

$$M = \beta(n) q^0(n) \left(\frac{q(n)}{q^0(n)} - \frac{q(n+1)}{q^0(n+1)} \right). \qquad \text{(A9)}$$

An expression for M in terms of $\Delta G(n)$ defined by eq. (A6) can be obtained by the repeated summation of eq. (A9),

$$\sum_{l=1}^{\infty} \left(\frac{q(l)}{q^0(l)} - \frac{q(l+1)}{q^0(l+1)} \right) = \frac{q(1)}{q^0(1)} - \frac{q(\infty)}{q^0(\infty)} = \sum_{l=1}^{\infty} \frac{M}{\beta_v(l) q^0(l)}. \qquad \text{(A10)}$$

We know, however, that $q(\infty)/q^0(\infty) \to 0$ and $q(1)/q^0(1) \to 1$ in analogy with classical nucleation theory [45]. Using eq. (A5) and noting that $q^0(1) = C_v$, the vacancy concentration, we obtain for the steady-state nucleation rate,

$$M = C_v / \sum_{n=1}^{\infty} \frac{\exp[\Delta G(n)/kT]}{\beta_v(n)}. \qquad \text{(A11)}$$

Eqs. (A6) and (A11) are the key relations which determine the steady-state nucleation rate.

The behavior of ΔG given by eq. (A6) is shown in fig. 5. The critical number of vacancies is defined corresponding to the peak in the curve by

$$\delta \Delta G(n)/\delta n = 0. \qquad \text{(A12)}$$

From eq. (A6) this becomes, for a change in the number of vacancies, δn, of unity,

$$0 = -kT \sum_{l=1}^{n} \ln \left(\frac{r_c(l) Z_v^c(l) D_v C_v}{r_c(l+1) Z_i^c(l+1) D_i C_i + r_c(l+1) Z_v^c(l+1) D_v C_v^c[r_c(l+1)]} \right) + kT \sum_{l=1}^{n-1} \ln \left(\frac{r_c(l) Z_v^c(l) D_v C_v}{r_c(l+1) Z_i^c(l+1) D_i C_i + r_c(l+1) Z_v^c(l+1) D_v C_v^c[r_c(l+1)]} \right), \qquad \text{(A13)}$$

or

$$\ln \left(\frac{r_c(n) Z_v^c(n) D_v C_v}{r_c(n+1) Z_i^c(n+1) D_i C_i + r_c(n+1) Z_v^c(n+1) D_v C_v^c[r_c(n+1)]} \right) = 0. \qquad \text{(A14)}$$

If we make the modest approximation that $r_c(n) \simeq r_c(n+1)$ this becomes

$$Z_v^c D_v C_v - Z_i^c D_i C_i - Z_v^c D_v C_v^c(r_c) = 0. \qquad \text{(A15)}$$

This is identical to eq. (10) with $dr_c/dt = 0$, the condition defining the critical radius in cavity growth theory. Note also that $C_v^c(r_c)$ is a general expression, given by eq. (11), allowing arbitrary gas pressure. This completes the proof of the equivalence of critical cavity radius, as well as stable cavity radius and critical number of gas atoms, in cavity growth theory and in cavity nucleation theory.

References

[1] N.M. Ghoniem, S. Sharafat, J.M. Williams and L.K. Mansur, J. Nucl. Mater. 117 (1983) 96.
[2] K. Farrell, P.J. Maziasz, E.H. Lee and L.K. Mansur, in: Int. Symp. on Helium in Metals, Julich, Germany (1982) to be published in Rad. Eff.
[3] S.D. Harkness and Che-Yu Li, Metall. Trans. 2 (1971) 1457.
[4] H. Wiedersich, Rad. Eff. 12 (1972) 111.
[5] A.D. Brailsford and R. Bullough, J. Nucl. Mater. 44 (1972) 121.

[6] G.W. Greenwood, A.J.E. Foreman and D.E. Rimmer, J. Nucl. Mater. 4 (1959) 305.
[7] K.C. Russell, Acta. Met. 26 (1978) 1615.
[8] A.D. Brailsford and R. Bullough, J. Nucl. Mater. 48 (1973) 87.
[9] V.F. Sears, J. Nucl. Mater. 39 (1971) 18.
[10] G.R. Odette and S.C. Langley, Proc. Int. Conf. on Radiation Effects and Tritium Technology for Fusion Reactors (October 1975) Gatlinburg, Tennessee, CONF-750989, eds., J.S. Watson and F.W. Wiffen, p. I-395.
[11] M.R. Hayns, M.H. Wood and R. Bullough, J. Nucl. Mater. 75 (1978) 241.
[12] N.M. Ghoniem and H. Gurol, Rad. Eff. 55 (1981) 209.
[13] S.B. Fisher, R.J. White and J.E. Harbottle, Rad. Eff. 40 (1979) 87.
[14] J.R. Townsend, J. Nucl. Mater. 108–109 (1982) 544.
[15] J.A. Spitznagel, W.J. Choyke, N.J. Doyle, R.B. Irwin, J.R. Townsend and J.N. McGruer, J. Nucl. Mater. 108–109 (1982) 537.
[16] A. Hishinuma and L.K. Mansur, J. Nucl. Mater., in press.
[17] R. Stoller and G.R. Odette, Effects on Radiation on Materials: Eleventh Conf., ASTM STP 782, eds., H.R. Brager and J.S. Perrin (Amer. Soc. for Testing and Materials, 1982) p. 275.
[18] L.K. Mansur, J. Nucl. Mater. 78 (1978) 156.
[19] M.R. Hayns and L.K. Mansur, in: Effects of Radiation on Materials: Tenth Conf., ASTM STP 725, eds., D. Kramer, H.R. Brager and J.S. Perrin (American Society for Testing and Materials, 1981) p. 213.
[20] L.K. Mansur, Nucl. Technol. 40 (1978) 5.
[21] L.K. Mansur, A.D. Brailsford and W.G. Wolfer, J. Nucl. Mater. 105 (1982) 36.
[22] W.A. Coghlan and L.K. Mansur, paper accepted for presentation at Third Topical Meeting on Fusion Reactor Materials, Albuquerque, NM (September 1983).
[23] C.A. Parker and K.C. Russell, Scripta Met. 15 (1981) 643.
[24] K.C. Russell, Acta Metall. 19 (1971) 753.
[25] J. Katz and H. Wiedersich, J. Chem. Phys. 55 (1971) 1414.
[26] W.G. Wolfer, L.K. Mansur and J.A. Sprague, Proc. Int. Conf. on Radiation Effects in Breeder Reactor Structural Materials (June 1977) Scottsdale, Arizona, eds., M.L. Bleiberg and J.W. Bennett (American Institute for Mining, Metallurgical and Petroleum Engineers, Inc.) p. 841.
[27] C.F. Clement and M.H. Wood, Proc. Roy. Soc. Lond. A371 (1980) 553.
[28] H. Trinkaus and H. Ullmaier, Phil. Mag. A39 (1979) 563.
[29] M.H. Yoo and L.K. Mansur, J. Nucl. Mater. 85–86 (1979) 571.
[30] D.J. Mazey and R.S. Nelson, J. Nucl. Mater. 85–86 (1979) 671.
[31] N.H. Packan, J. Nucl. Mater. 103–104 (1981) 1029.
[32] G.R. Odette and M.W. Frei, Proc. First Topical Mtg. on the Tech. of Controlled Nuclear Fusion (April 1974) San Diego, California, CONF-740402-P2.
[33] M.R. Hayns and M.H. Wood, J. Nucl. Mater. 87 (1979) 97.
[34] L.K. Mansur, P.R. Okamoto, A. Taylor and Che-Yu Li, Proc. Int. Conf. on Defects and Defect Clusters in B.C.C. Metals and Their Alloys (1973) ed., R.J. Arsenault, p. 509.
[35] W.G. Wolfer and L.K. Mansur, J. Nucl. Mater. 91 (1980) 265.
[36] E.H. Lee, private communication.
[37] E.A. Kenik and E.H. Lee, Proc. Electron Microscopy Society of America, 41st Annual Meeting (1983) ed., G.W. Bailey (Claitor's Publishing Division).
[38] L.K. Mansur, K. Farrell and J.O. Stiegler, Trans. Amer. Nucl. Soc., Tansao 21 (1975) 163.
[39] J.L. Brimhall and L.A. Charlot, J. Nucl. Mater. 99 (1981) 16.
[40] K. Farrell, Rad. Eff. 53 (1980) 175.
[41] N.H. Packan and K. Farrell, J. Nucl. Mater. 85–86 (1979) 677.
[42] E.H. Lee, A.F. Rowcliffe and L.K. Mansur, J. Nucl. Mater. 103–104 (1981) 1475.
[43] L.K. Mansur, Phil. Mag. 44A (1981) 867.
[44] S.A. Seyyedi, K.C. Russell and M. Hadji-Mirgai, in: Proc. of Int. Conf. on Irradiation Behavior of Metallic Materials for Fast Reactor Core Components (June 1979) Corsica, France, eds., J. Poirier and J.M. DuPouy, (Le Commissariat a L'Energie Atomique) p. 101.
[45] J.W. Christian, The Theory of Transformations in Metals and Alloys, Part I, Second Ed. (Pergamon Press, New York, 1975).
[46] E.A. Kenik and E.H. Lee, in: Phase Stability during Irradiation, eds., J.R. Holland, L.K. Mansur and D.J. Potter, Proc. Symp. (October 1980) Pittsburgh, PA (The Metallurgical Society of AIME) p. 493.
[47] A.F. Rowcliffe and E.H. Lee, J. Nucl. Mater. 108–109 (1982) 306.
[48] P.J. Maziasz, J. Nucl. Mater. 108–109 (1982) 359.
[49] P.J. Maziasz, private communication.
[50] H.R. Brager and F.A. Garner, J. Nucl. Mater. 103–104 (1981) 993.
[51] L.K. Mansur and W.G. Wolfer, Oak Ridge National Laboratory Report, ORNL/TM-5670 (1977).